SECURITY INFORMATION

CONFIDENTIAL

329

Copy
RM L52G08a

NACA RM L52G08a

NACA

CASE FILE
COPY

RESEARCH MEMORANDUM

INVESTIGATION OF THE LOW-SPEED AERODYNAMIC CHARACTERISTICS OF A VARIABLE-SWEEP AIRPLANE MODEL WITH A WING HAVING PARTIAL-SPAN CAMBERED-LEADING-EDGE MODIFICATIONS

By Robert E. Becht and Andrew L. Byrnes, Jr.

Langley Aeronautical Laboratory
Langley Field, Va.

CLASSIFICATION CHANGED TO UNCLASSIFIED

AUTHORITY: NACA RESEARCH ABSTRACT NO. 94

DATE: JAN 11, 1956 WHL

CLASSIFIED DOCUMENT

This material contains information affecting the National Defense of the United States within the meaning of the espionage laws, Title 18, U.S.C., Secs. 793 and 794, the transmission or revelation of which in any manner to unauthorized person is prohibited by law.

NATIONAL ADVISORY COMMITTEE
FOR AERONAUTICS

WASHINGTON
September 16, 1952

CONFIDENTIAL

NATIONAL ADVISORY COMMITTEE FOR AERONAUTICS

RESEARCH MEMORANDUM

INVESTIGATION OF THE LOW-SPEED AERODYNAMIC CHARACTERISTICS OF A VARIABLE-SWEEP AIRPLANE MODEL WITH A WING HAVING PARTIAL-SPAN CAMBERED-LEADING-EDGE MODIFICATIONS

By Robert E. Becht and Andrew L. Byrnes, Jr.

SUMMARY

An investigation was made to determine the aerodynamic characteristics at low speed of a variable-sweep airplane model with a wing having cambered sections outboard of the 40-percent-semispan station at 50° sweep and ahead of the 45-percent streamwise chord line. Two leading-edge camber designs were tested, one having twice the camber of the other. A comparison was made with the data obtained on the same model incorporating a wing of symmetrical sections and also a fully cambered and twisted wing. The effect of partial-span split flaps on the wing at 20° sweep was also included in the investigation.

The results of the investigation, which was made at a Reynolds number of 2×10^6 based on the mean aerodynamic chord at 50° sweep, indicated that the effects of the leading-edge-camber modifications were similar to those obtained with a fully cambered and twisted wing.

The highest value of tail-off maximum lift coefficient was obtained at all sweep angles from the wing section having the maximum leading-edge camber. The flap effectiveness at the minimum sweep angle of 20° was about equal for all configurations. At sweep angles in excess of about 35°, the partial-span leading-edge-camber modifications were not as effective as the fully cambered and twisted wing in increasing the maximum lift-drag ratio $(L/D)_{max}$ of the symmetrical wing model. In addition, the fully cambered and twisted wing generally had the highest L/D values at lift coefficients above that corresponding to $(L/D)_{max}$ for all sweep angles.

INTRODUCTION

Previous investigations of the aerodynamic characteristics of a $\frac{1}{4}$-scale model, representative of the Bell X-5 airplane, have shown that appreciable performance gains were obtained when a fully cambered and twisted wing was used on the model in place of a wing having symmetrical sections. (See refs. 1, 2, 3, and 4.) Inasmuch as the fully cambered and twisted wing used in reference 3 would require curved hinge lines for the control surfaces and would also further complicate the wing-fuselage juncture problems on a variable-swept-wing aircraft, a more practical wing design that would retain at least some of these performance gains was desirable.

The present paper contains the results of an investigation at low speed of the same model as used previously, but with a wing having two interchangable partial-span leading-edge-camber modifications. Data are presented for each of the leading-edge modifications at wing sweep angles of 20°, 35°, 50°, and 60°. The effect of partial-span split flaps was obtained at only the minimum sweep angle of 20°.

SYMBOLS

The system of axes employed, together with the positive direction of the forces, moments, and angles, is given in figure 1. The aerodynamic force and moment coefficients are based on the actual wing area and span which vary with sweep angle, but a constant chord, equal to the wing mean aerodynamic chord at 50° sweep, is used for the pitching-moment coefficients. The pitching moments were measured about a fixed fuselage station corresponding to the quarter-chord point of the mean aerodynamic chord of the wing, which was translated so that the quarter-chord point of the mean aerodynamic chord at any sweep angle fell at this same fuselage station. (See fig. 2.) The symbols used are defined as follows:

C_L lift coefficient, Lift/qS

C_X longitudinal-force coefficient, X/qS

C_Y lateral-force coefficient, Y/qS

C_l rolling-moment coefficient, L/qSb

C_m	pitching-moment coefficient, $M/qS\bar{c}_{50}$
C_n	yawing-moment coefficient, N/qSb
X	longitudinal force along X-axis (Drag = -X), lb
Y	lateral force along Y-axis, lb
Z	force along Z-axis (Lift = -Z), lb
L	rolling moment about X-axis, ft-lb
M	pitching moment about Y-axis, ft-lb
N	yawing moment about Z-axis, ft-lb
L/D	ratio of lift to drag
q	free-stream dynamic pressure, $\rho V^2/2$, lb/sq ft
ϵ	effective downwash angle at the tail, deg
S	wing area, sq ft
$\bar{c}$	wing mean aerodynamic chord, $\dfrac{\int_0^{b/2} c^2 dy}{\int_0^{b/2} c\, dy}$, ft; based on plan forms shown in fig. 2
$\bar{c}_{50}$	wing mean aerodynamic chord at 50° sweep, ft
c'	local streamwise wing chord, ft
c	local wing chord perpendicular to quarter-chord line of unswept wing, ft
b	wing span, ft
V	free-stream velocity, fps
A	aspect ratio, b^2/S
ρ	mass density of air, slugs/cu ft

α angle of attack of thrust line, deg

β angle of sideslip, deg

i_t angle of incidence of stabilizer with respect to thrust line, deg

δ_f flap deflection measured in a plane perpendicular to hinge line, deg

Λ angle of sweepback of quarter-chord line of unswept wing, deg

y spanwise distance measured perpendicular from plane of symmetry, ft

z height above chord plane of symmetrical sections

d streamwise distance back of local wing leading edge, ft

Subscripts:

β denotes partial derivative of a coefficient with respect to sideslip angle; for example, $C_{l_\beta} = \frac{\partial C_l}{\partial \beta}$

max maximum

APPARATUS AND MODEL

Description of Model

The physical characteristics of the model are presented in figure 2 and photographs of the model on the support strut are given in figure 3. Figure 4 shows the details of the split flap. The model was constructed of wood bonded to steel reinforcing members.

The model used in the present investigation was the same as that used in the tests of references 1, 2, and 3 with the exception of the wing sections. The wing sections inboard of the 40-percent-semispan station and behind the 45-percent-chord line outboard of this spanwise station were the same as that used in references 1 and 2. The remaining portion of the wing was designed to have the same camber as the wing used in reference 3 for modification 1 and twice this camber for modification 2. (The wing used in ref. 3 was cambered and twisted so as

to produce a uniform load distribution at a Mach number of 1.10 and a lift coefficient of 0.25 for the wing at 50° sweep.) A plot of the modified camber line at two semispan stations of the 50° swept wing is presented in figure 5 for the two camber designs investigated. The thickness distribution measured in planes normal to the 0.25-chord line of the unswept panel was NACA $64_{(10)}$-010.3 at the root tapering to NACA 64-008 at the tip.

The wings were pivoted about axes parallel to the plane of symmetry and normal to the chord-plane inboard of the 40-percent-semispan station at 50° sweep so that the sweepback angle could be varied continuously from 20° to 60°. The incidence of this chord plane measured in a streamwise direction was zero.

A jet-engine duct was simulated on the model by use of an open tube having an inside diameter equal to that of the jet exit and extending from the nose to the jet exit.

TESTS

The tests were made in the Langley 300 MPH 7- by 10-foot tunnel at a dynamic pressure of 34.15 pounds per square foot which corresponds to a Mach number of 0.152 and a Reynolds number of 2×10^6 based on the mean aerodynamic chord at 50° sweep for average test conditions.

During the tests, no control was imposed on the quantity of air flow through the jet duct. Measurements made in previous tests indicated that the inlet velocity ratio varied between 0.78 and 0.86, the higher values being observed at low angles of attack.

The effective downwash was calculated from the pitching-moment results by using various horizontal tail settings. The parameters C_{n_β}, C_{Y_β}, and C_{l_β} were determined from tests through the angle-of-attack range at sideslip angles of 0° and -5°.

CORRECTIONS

The angle-of-attack, drag, and pitching-moment results have been corrected for jet-boundary effects that were computed on the basis of an unswept wing theory by the method of reference 5. All coefficients have been corrected for blocking due to the model and its wake by the method of reference 6.

Corrections for the tare forces and moments produced by the support strut have not been applied. It is probable, however, that the significant tare corrections would be limited to small increments in pitching moment and drag.

Vertical buoyancy on the support strut, tunnel air-flow misalinement, and the longitudinal pressure gradient have been accounted for in computation of the test data.

RESULTS AND DISCUSSION

Presentation of Results

The results of the investigation are presented in the figures listed as follows:

	Figure
Longitudinal aerodynamic characteristics	6 and 7
Effect of flaps on the longitudinal aerodynamic characteristics	8
$C_{L_{max}}$ comparisons	9
Drag comparisons	10
Lift-drag ratios	11 and 12
Pitching-moment comparisons	13
Effective downwash	14
Lateral and directional stability characteristics	15

In order to provide a comparison which will indicate the effects of the leading-edge camber modifications, data from references 1 and 2 on the same model but with a wing having symmetrical sections are included in some of the figures. In addition, data are presented from reference 3 for the same model but with a fully cambered and twisted wing which was designed to produce a uniform load distribution at a Mach number of 1.10 and a lift coefficient of 0.25 for the wing at 50° sweep. As previously mentioned in the section on symbols, the aerodynamic coefficients presented herein are based on the wing area and span of the sweep in question and on the mean aerodynamic chord of the wing at 50° sweep. The pitching-moment coefficients are, thus, based on a reference length which is fixed with respect to the fuselage, whereas all other coefficients are of the usual form.

Basic Characteristics

In general, the leading-edge modifications produced the same trends in the aerodynamic characteristics of the model as the fully cambered and twisted wing. Inasmuch as a detailed discussion of these trends may be found in reference 3, the present discussion will be limited. The model configuration with the symmetrical wing (refs. 1 and 2) will be used as the basis for comparison of the aerodynamic effects of the two leading-edge modifications and the fully cambered and twisted wing (ref. 3).

Lift and Drag Characteristics

The summary of maximum lift coefficients presented in figure 9 shows that the leading-edge-camber modification 2 had the highest value at all sweep angles and modification 1 had values greater than those of the fully cambered and twisted wing at sweep angles in excess of about 45°. It can also be seen in figure 9 that the gain in maximum lift coefficient produced by deflecting the partial-span split flaps was about equal for all model configurations at 20° sweep.

The leading-edge-camber modification 2 was almost as effective in reducing drag due to lift as the fully cambered and twisted wing at all sweep angles. (See fig. 10.) As might be anticipated from the camber difference, the modification 1 was less effective.

In figures 11 and 12 it can be seen that for sweep angles very near 20° the cambered leading-edge modification 1 had the highest $(L/D)_{max}$ of the wing plan forms reported herein; at sweep angles in excess of about 35°, the fully cambered and twisted wing had the highest $(L/D)_{max}$. Moreover, the fully cambered and twisted wing generally was more effective at all sweep angles in increasing the L/D values at lift coefficients above that corresponding to $(L/D)_{max}$.

Pitching-Moment Characteristics

The summary of tail-off pitching-moment coefficients for each model configuration (fig. 13) shows that at all sweep angles the model with the cambered leading-edge modifications had much smaller nose-down pitching moments at zero lift than the fully cambered and twisted wing model. The effect of sweep, in general, was to reduce the magnitude of the zero-lift pitching-moment coefficient. At 50° and 60° sweep, the model with any of the wings investigated showed an increase in stability at an intermediate lift coefficient followed by a decrease in stability

at high lift coefficients. The effect of the cambered leading-edge modifications was to increase the lift coefficient (beyond that of the symmetrical wing) at which these stability changes occurred. At low lift coefficients, none of the wing modifications had any appreciable effect on the longitudinal stability of the model. As shown by figure 14, the effective downwash at the tail was essentially unchanged by the cambered leading-edge modifications, probably because the span of the inboard symmetrical sections and the span of the tail were very nearly equal.

Lateral Stability Characteristics

The lateral stability parameters presented in figure 15 show that at sweep angles less than 50°, the leading-edge-camber modifications increased the effective dihedral $-C_{l_\beta}$ at high lift coefficients. This effect is similar to that produced by the fully cambered and twisted wing. The directional instability observed at high lift coefficients of the model with the symmetrical wing was attributed in reference 2 to mutual interference between wing, fuselage, and tail. The use of either the cambered leading-edge modifications or the fully cambered and twisted wing increased the lift coefficient at which directional instability occurred; but the incremental difference between the lift coefficient for stall and lift coefficient for directional instability was approximately the same for all model configurations. In all other respects, the trends in the lateral and directional stability characteristics were essentially unchanged by the leading-edge-camber modifications.

CONCLUSIONS

The results of the present investigation of partial-span leading-edge-camber modifications compared to the results obtained on the same model but with a wing of symmetrical sections as one limit and a fully cambered and twisted wing as the other, indicate the following conclusions:

1. In general, both cambered leading-edge modifications produced the same trends in the aerodynamic characteristics of the model as the fully cambered and twisted wing.

2. The highest value of tail-off maximum lift coefficient was obtained at all sweep angles from leading-edge camber modification 2 (which had twice the camber of modification 1).

3. The flap effectiveness at the minimum sweep angle of 20° was about equal for all configurations.

4. The reduction in drag due to lift was about the same for the model with either the leading-edge-camber modification 2 or the fully cambered and twisted wing.

5. At sweep angles in excess of about 35°, the partial-span leading-edge-camber modifications were not as effective as the fully cambered and twisted wing in increasing the maximum lift-drag ratio $(L/D)_{max}$ of the symmetrical wing model. In addition, the fully cambered and twisted wing generally had the highest L/D values at lift coefficients above that corresponding to $(L/D)_{max}$ for all sweep angles.

6. The lateral and directional stability trends were essentially the same as previously reported for the fully cambered and twisted wing.

Langley Aeronautical Laboratory
National Advisory Committee for Aeronautics
Langley Field, Va.

REFERENCES

1. Kemp, William B., Jr., Becht, Robert E., and Few, Albert G., Jr.: Stability and Control Characteristics at Low Speed of a $\frac{1}{4}$-Scale Bell X-5 Airplane Model. Longitudinal Stability and Control. NACA RM L9K08, 1950.

2. Kemp, William B., Jr., and Becht, Robert E.: Stability and Control Characteristics at Low Speed of a $\frac{1}{4}$-Scale Bell X-5 Airplane Model. Lateral and Directional Stability and Control. NACA RM L50C17a, 1950.

3. Kemp, William B., Jr., Becht, Robert E., and Few, Albert G., Jr.: Investigation of the Low-Speed Aerodynamic Characteristics of a Variable-Sweep Airplane Model With a Twisted and Cambered Wing. NACA RM L51K22, 1952.

4. Alford, William J., Jr., and Byrnes, Andrew L., Jr.: Small-Scale Transonic Investigation of the Effects of Partial-Span Leading-Edge Camber on the Aerodynamic Characteristics of a 50° 38' Swept-back Wing of Aspect Ratio 2.98. NACA RM L52D08a, 1952.

5. Gillis, Clarence L., Polhamus, Edward C., and Gray, Joseph L., Jr.: Charts for Determining Jet-Boundary Corrections for Complete Models in 7- by 10-Foot Closed Rectangular Wind Tunnels. NACA ARR L5G31, 1945.

6. Herriot, John G.: Blockage Corrections for Three-Dimensional-Flow Closed-Throat Wind Tunnels, With Consideration of the Effect of Compressibility. NACA Rep. 995, 1950. (Supersedes NACA RM A7B28.)

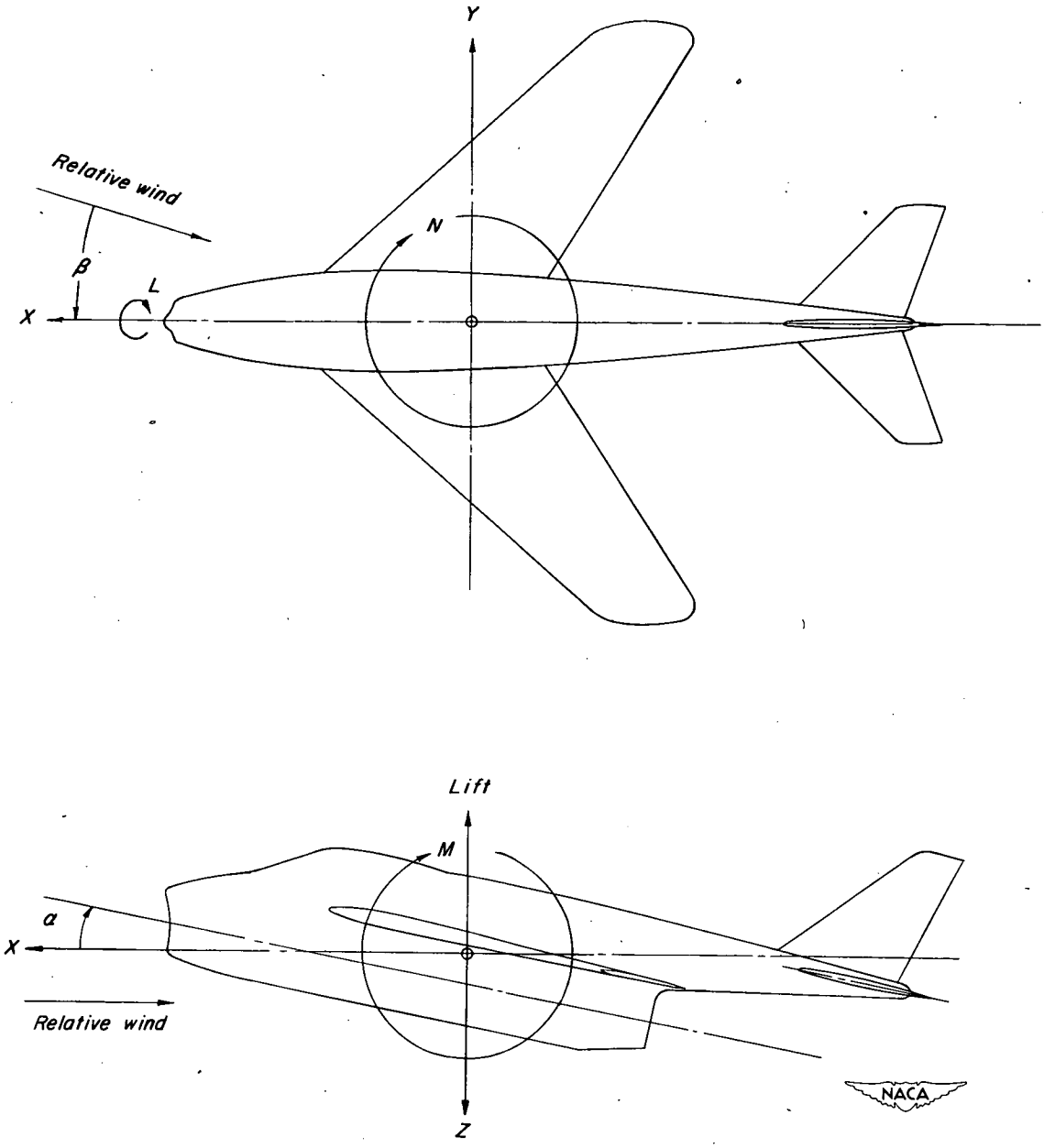

Figure 1.- System of axes. Positive directions of forces, moments, and angles are indicated by arrows.

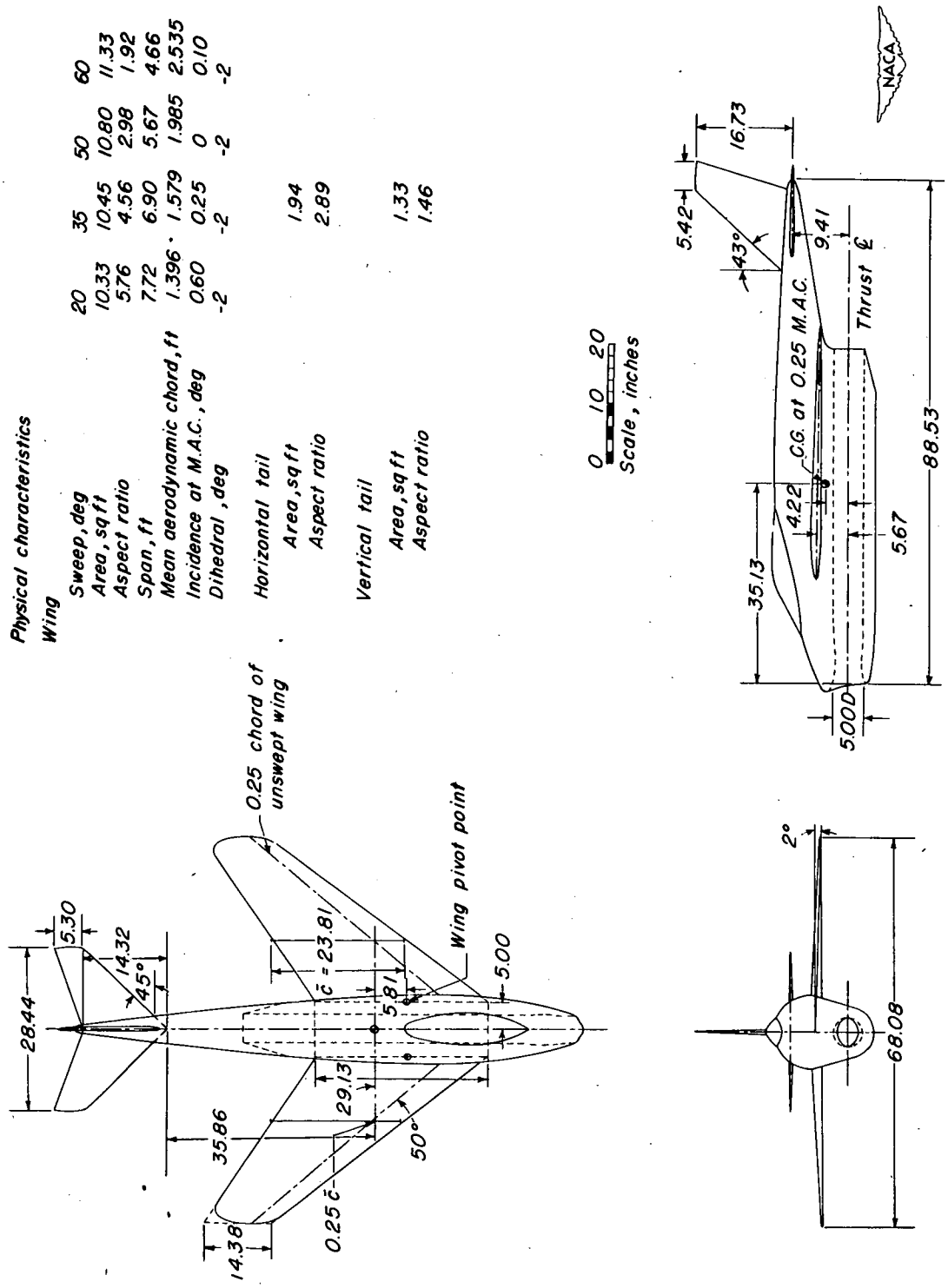

Figure 2.- General arrangement of test model.

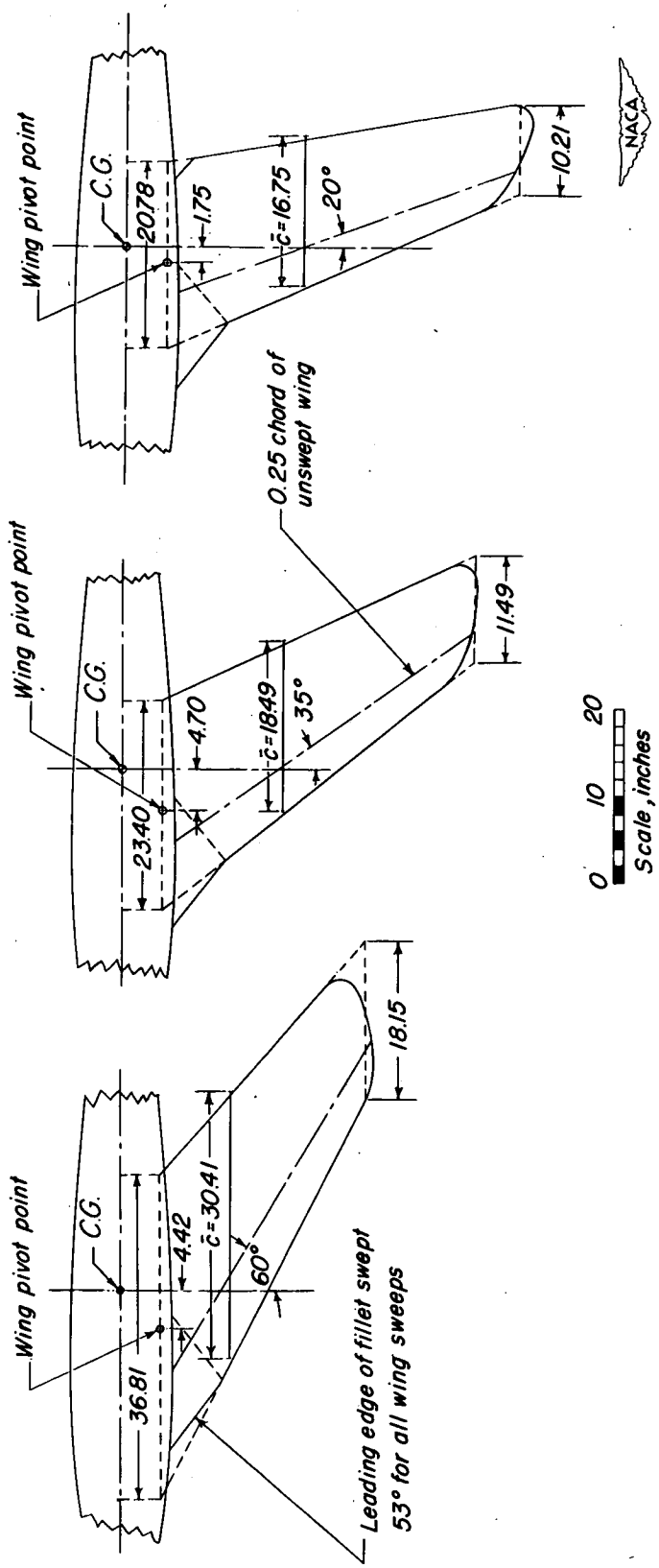

Figure 2.- Concluded.

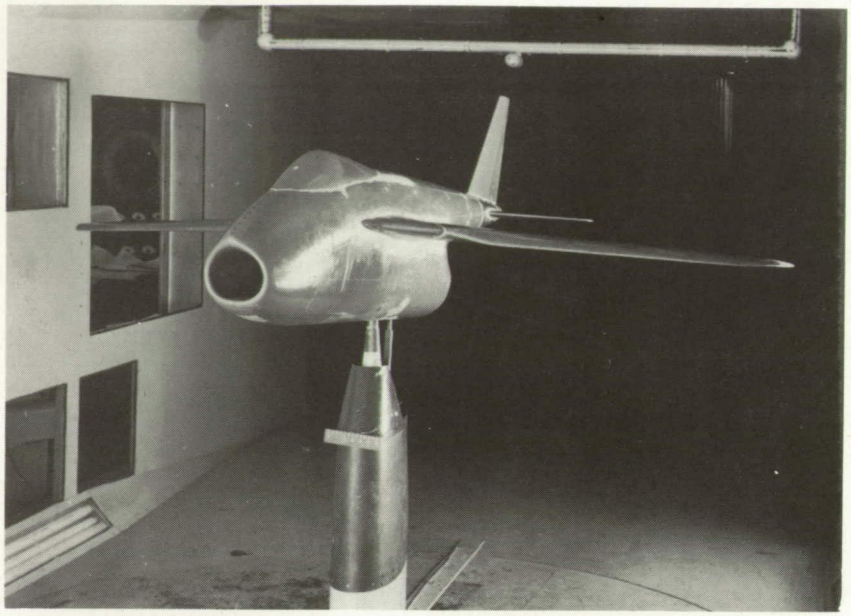

(a) $\Lambda = 20^{\circ}$.

NACA
L-71866

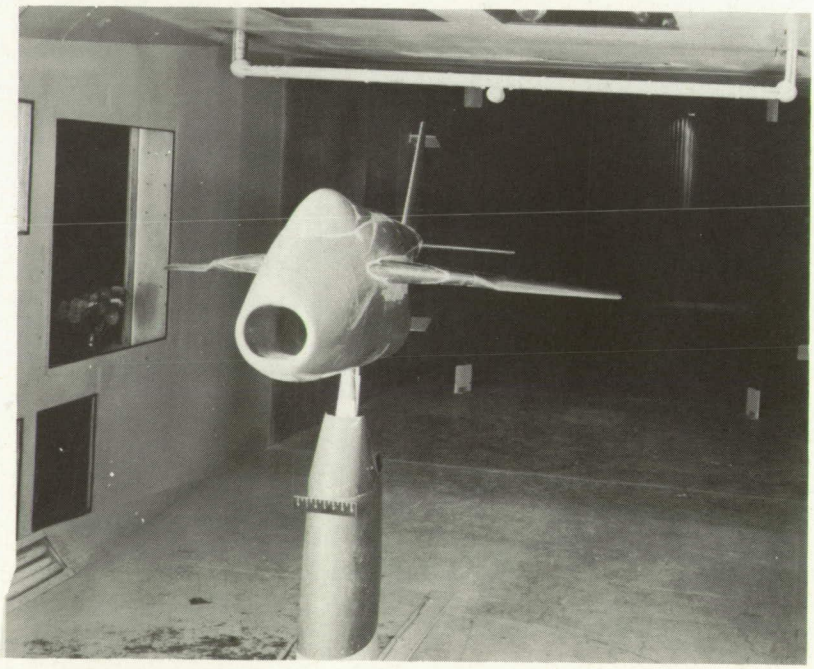

(b) $\Lambda = 60^{\circ}$.

NACA
L-72114

Figure 3.- Views of test model as mounted on support strut in tunnel with leading-edge-camber modification 2.

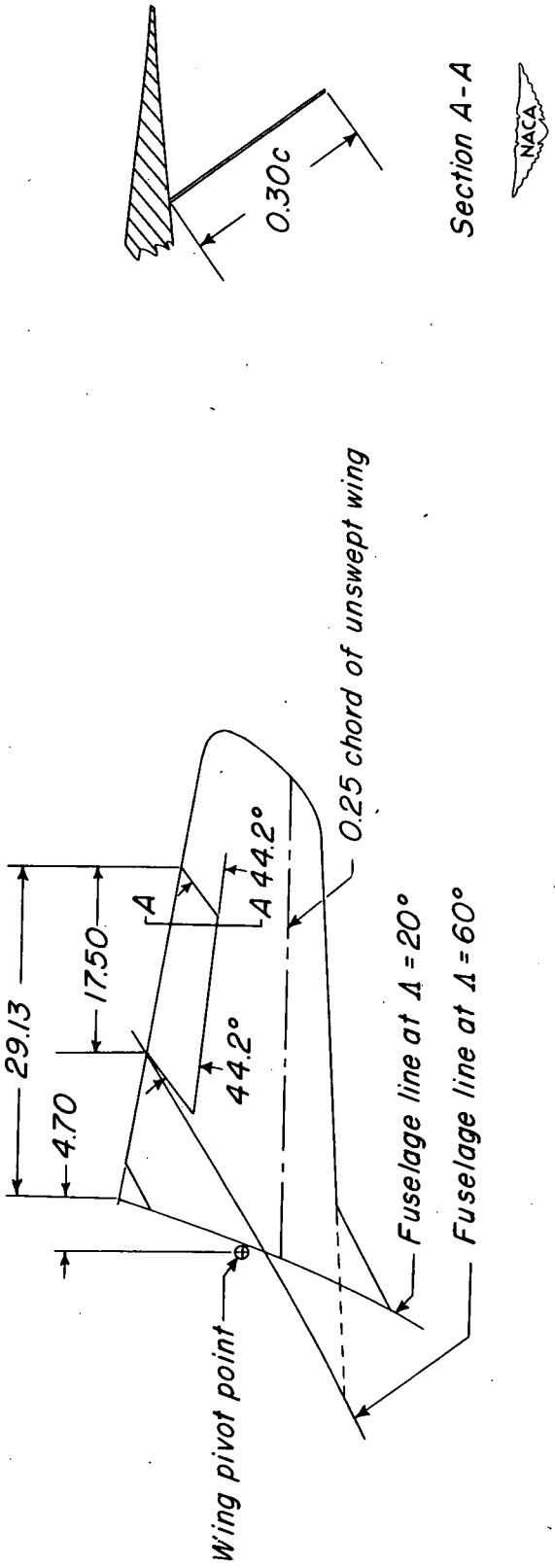

Figure 4.- Details of split flap.

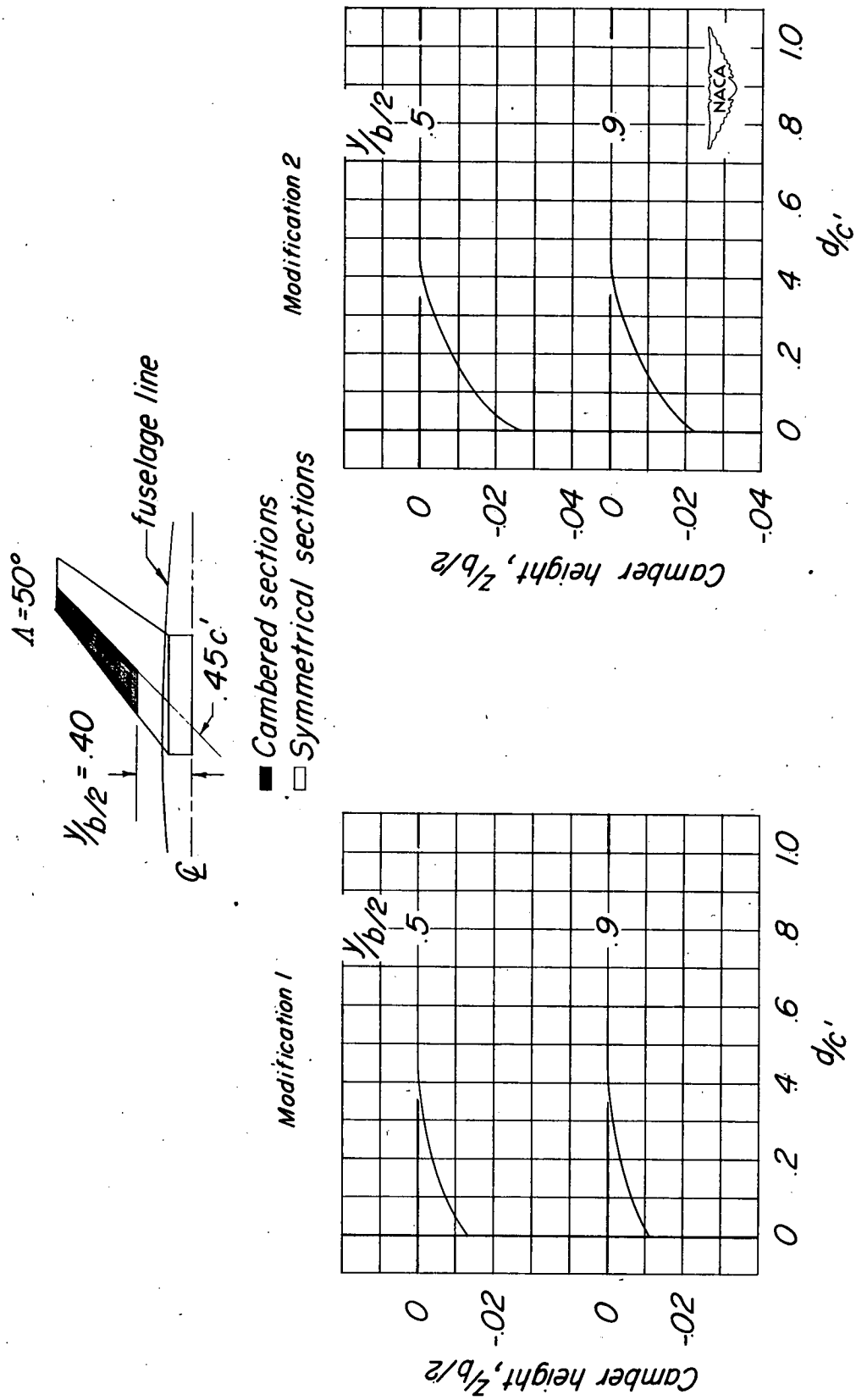

Figure 5.- Variation of wing mean camber height with streamwise chord at 50° sweep.

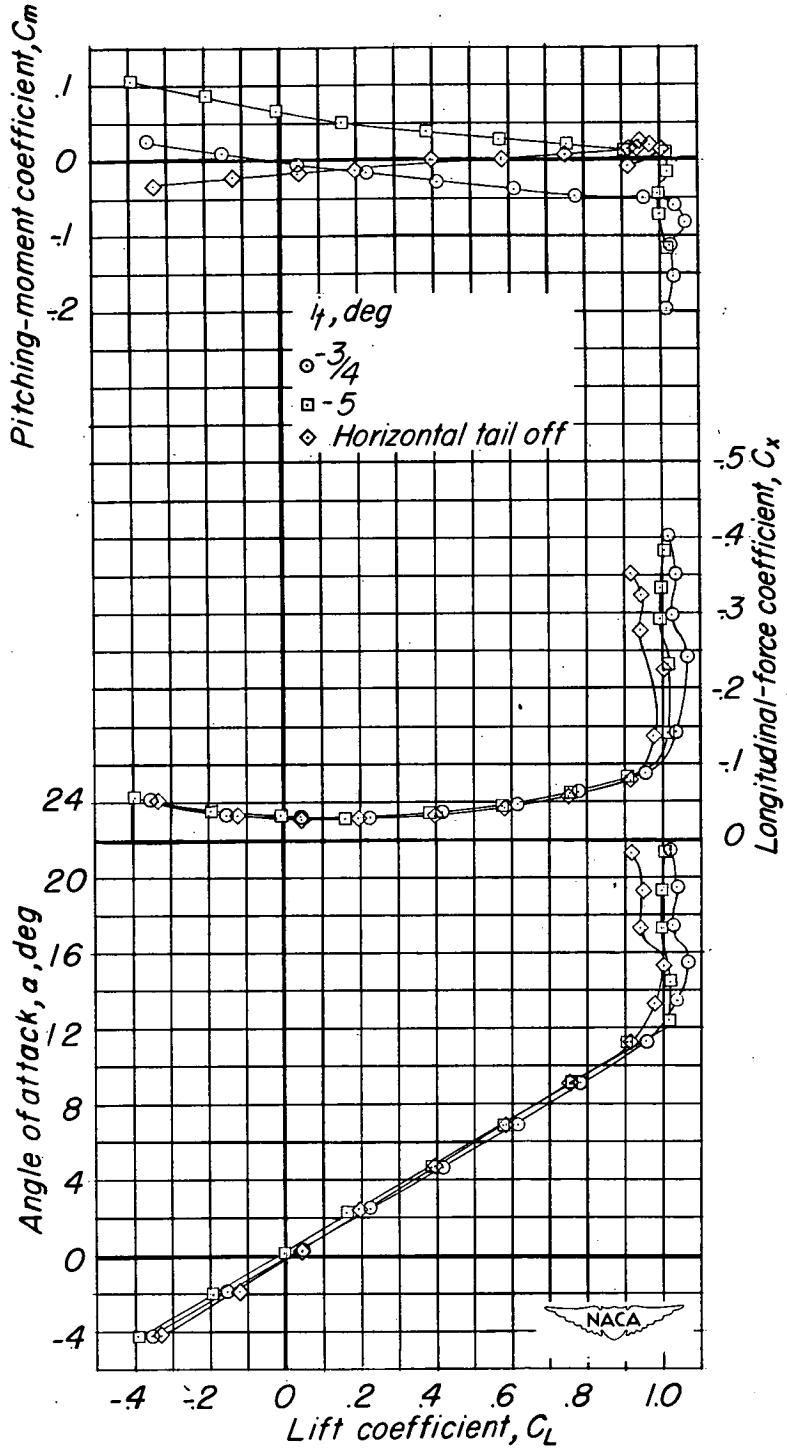

(a) $\Lambda = 20^{\circ}$.

Figure 6.- Longitudinal aerodynamic characteristics of the model with modification 1. $\delta_f = 0$.

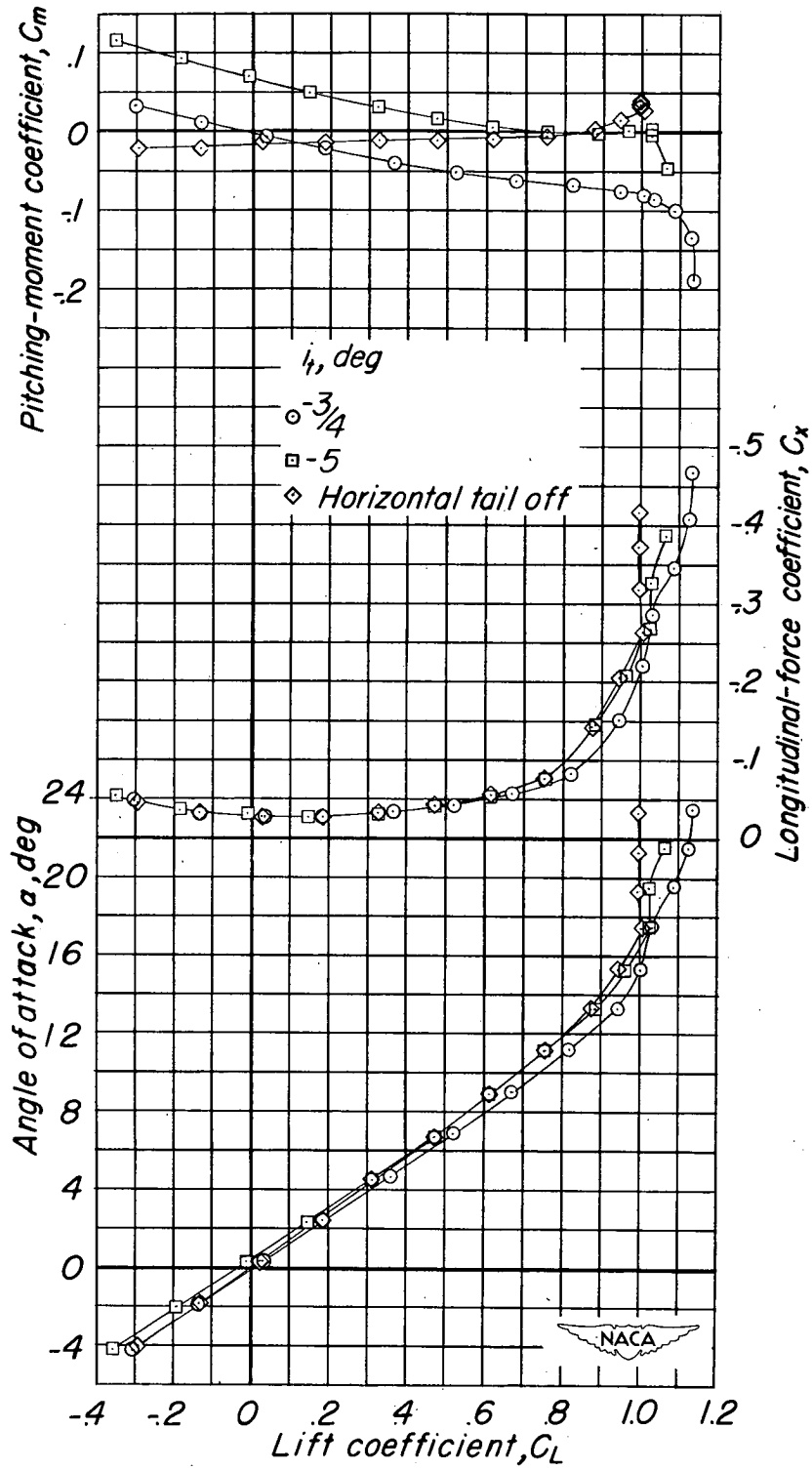

(b) $\Lambda = 35^{\circ}$.

Figure 6.- Continued.

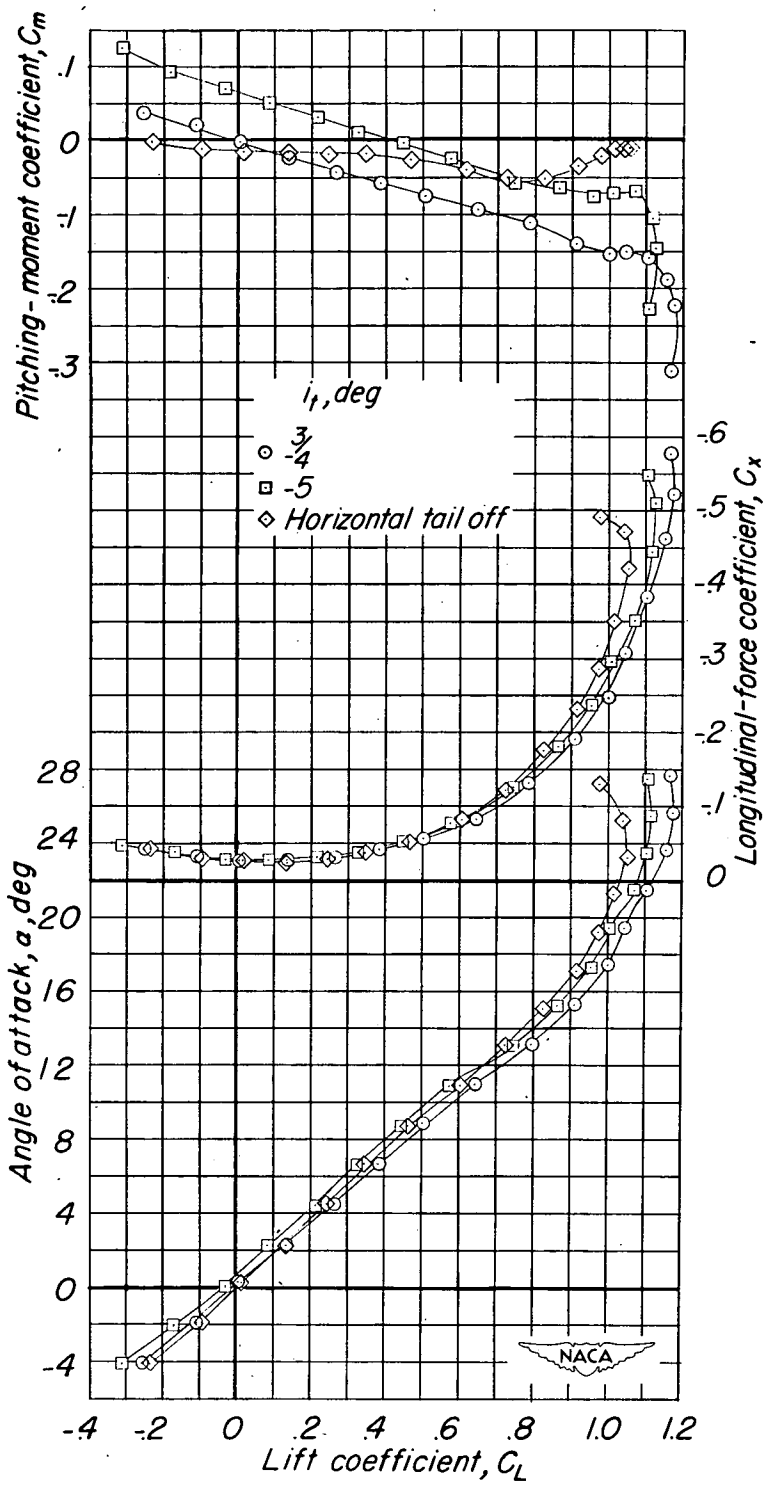

(c) $\Lambda = 50^{\circ}$.

Figure 6.- Continued.

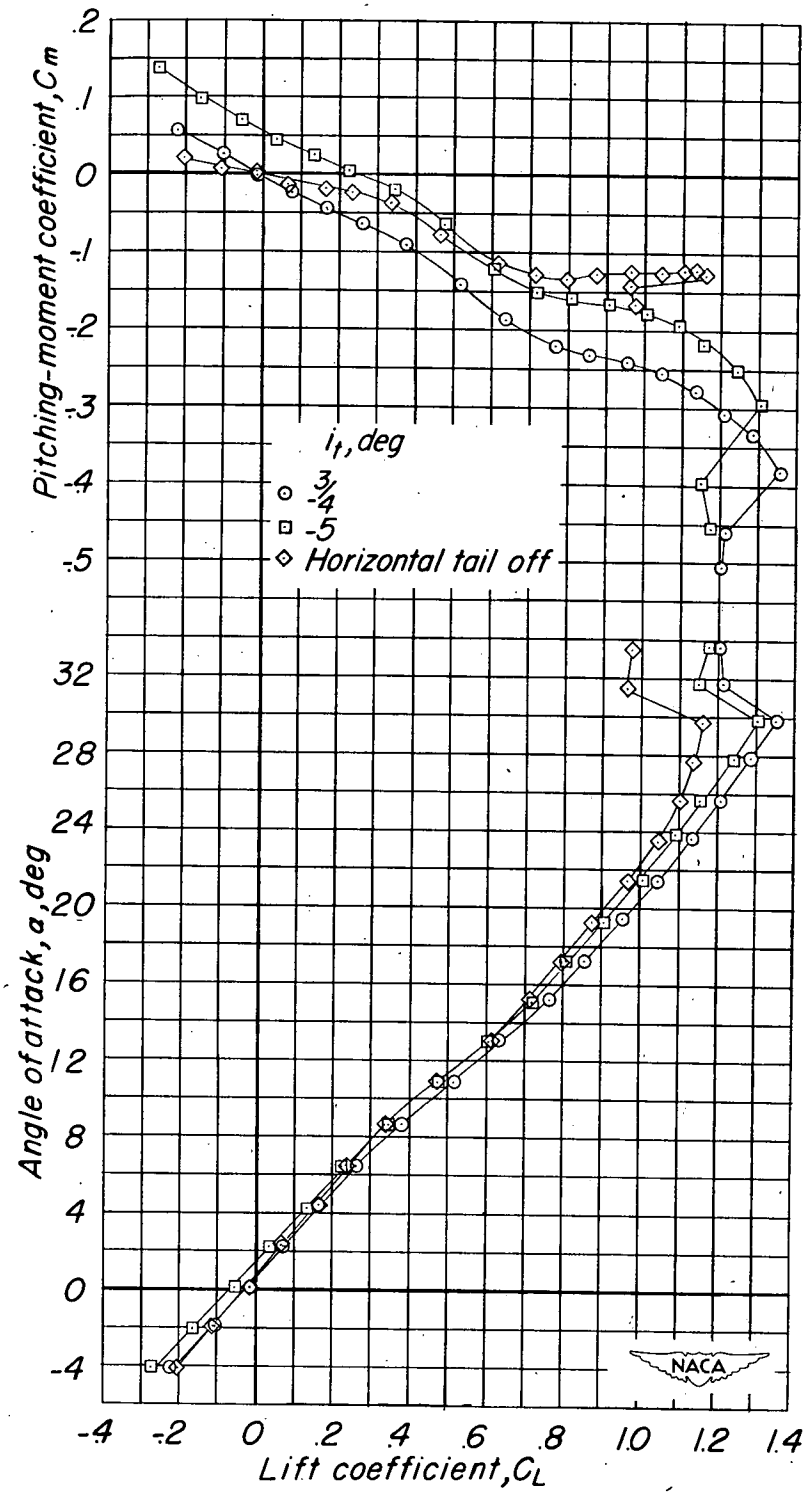

(d) $\Lambda = 60^{\circ}$.

Figure 6.- Continued.

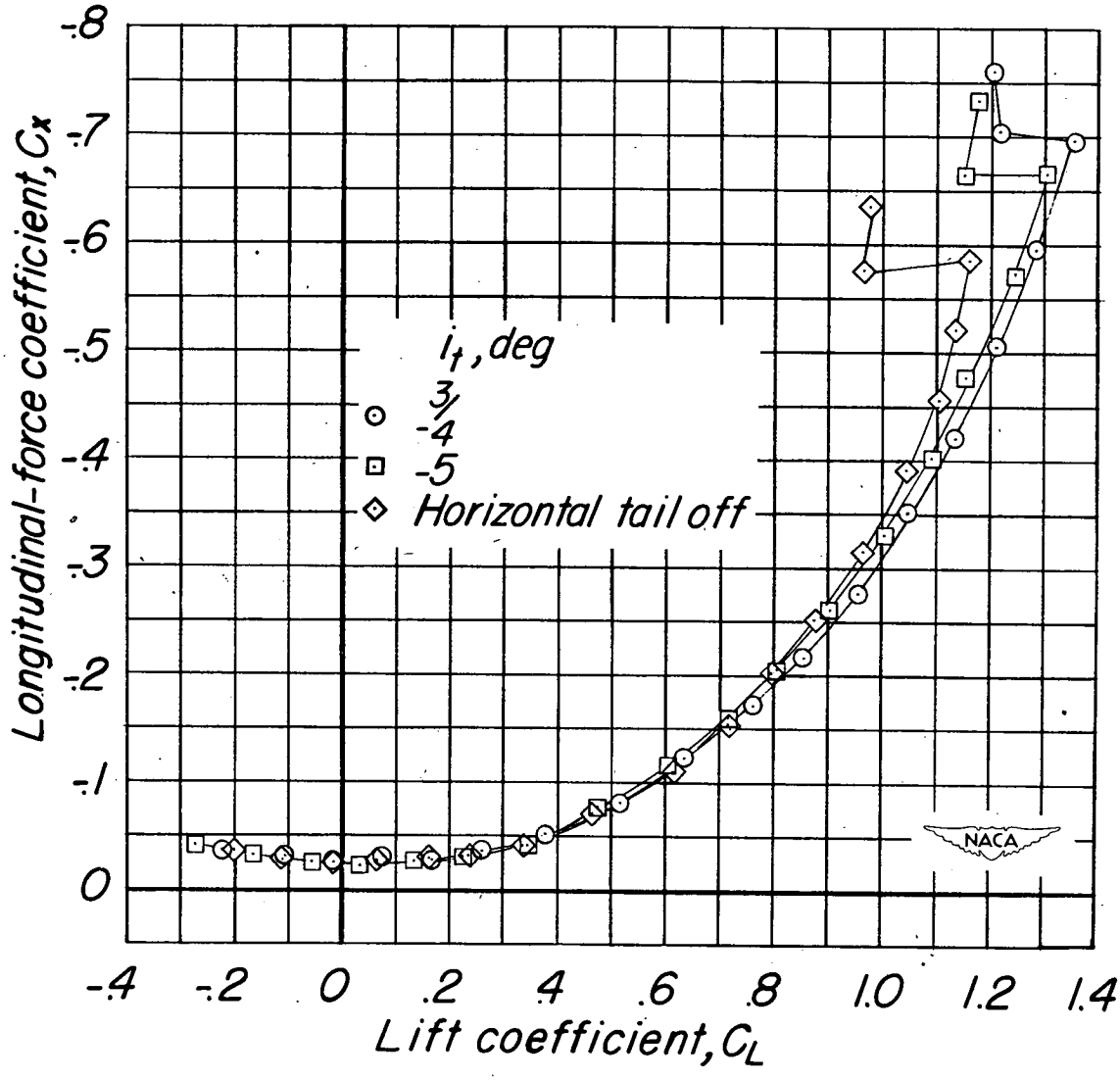

(d) Concluded.

Figure 6.- Concluded.

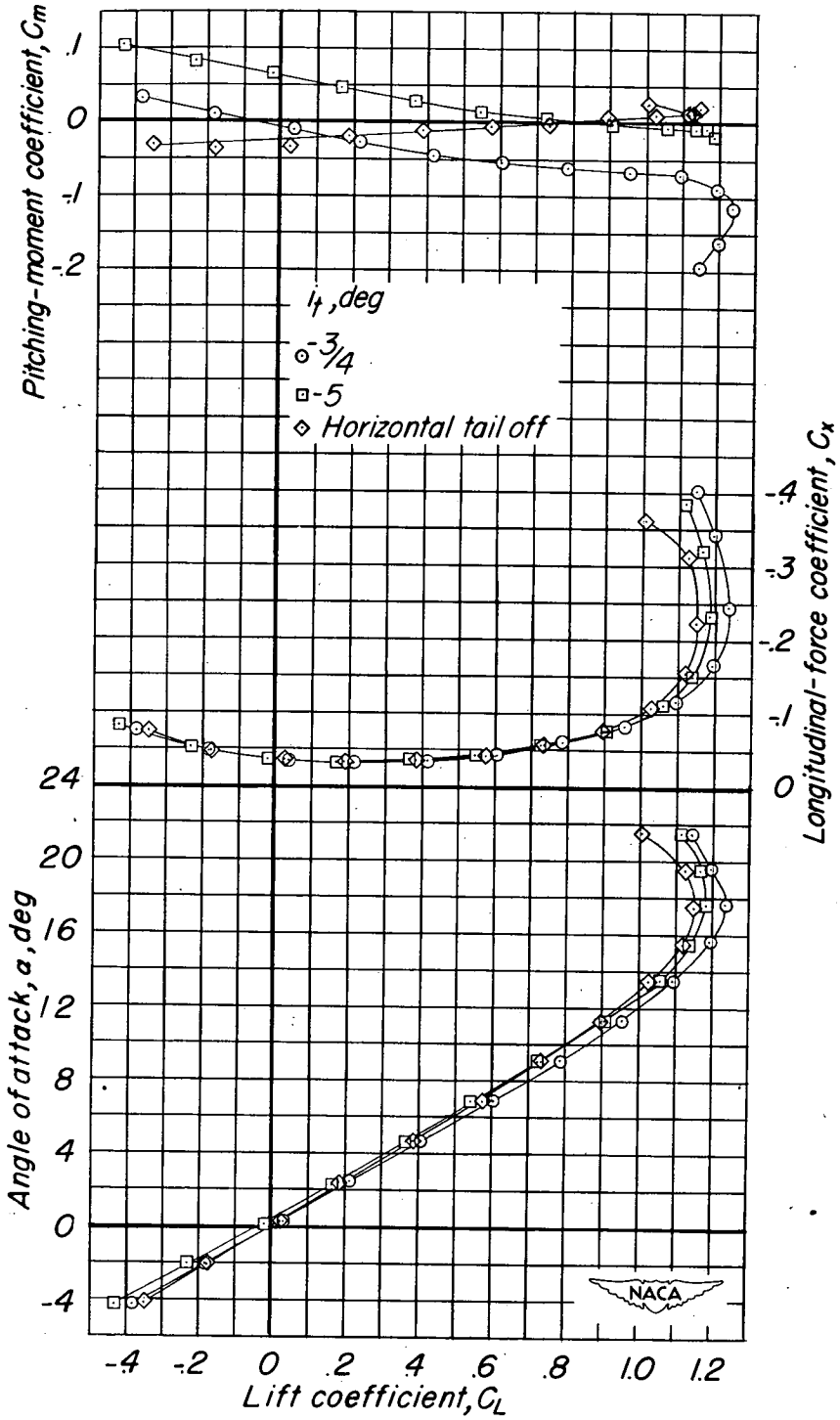

(a) $\Lambda = 20^{\circ}$.

Figure 7.- Longitudinal aerodynamic characteristics of the model with modification 2. $\delta_f = 0$.

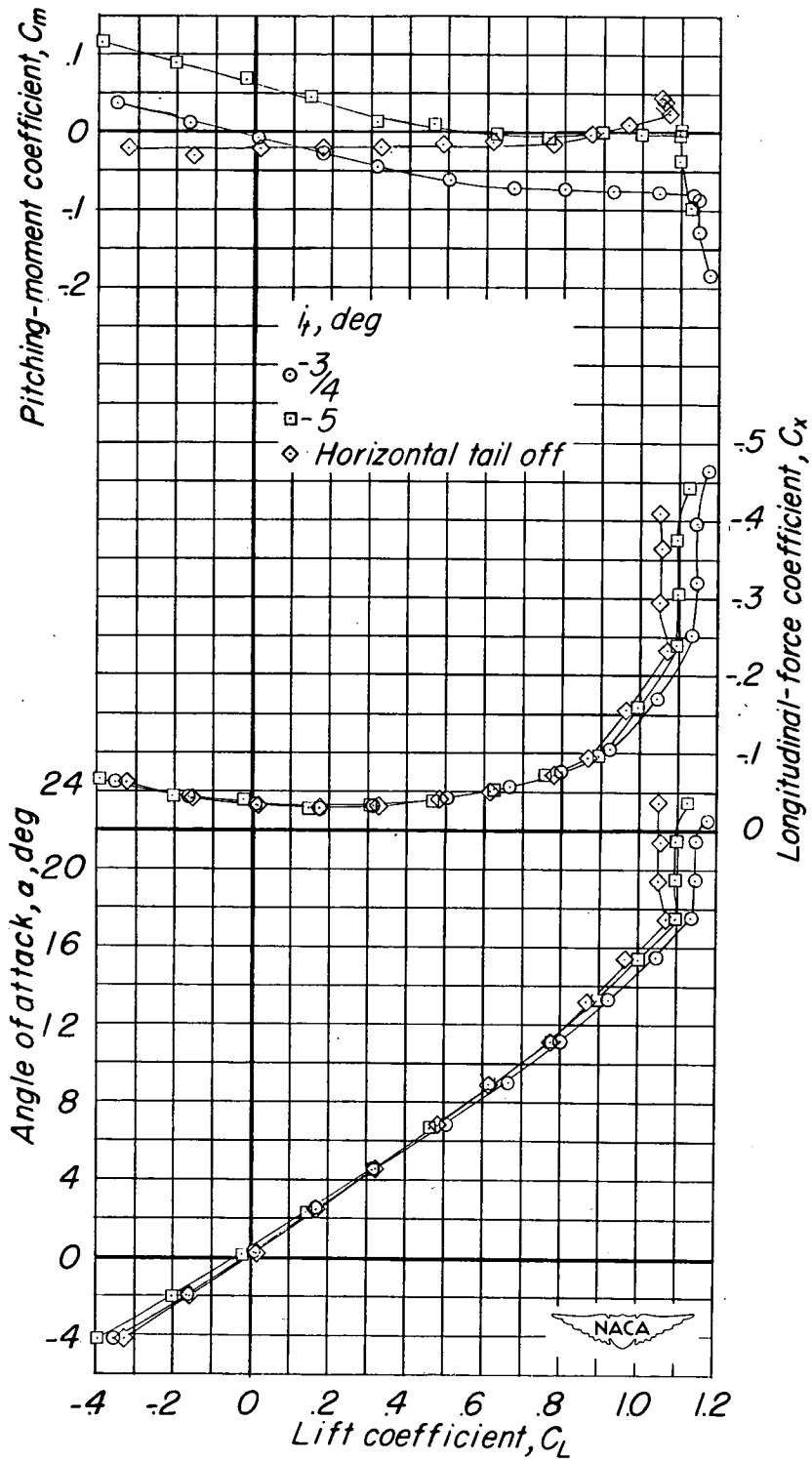

(b) $\Lambda = 35^{\circ}$.

Figure 7.- Continued.

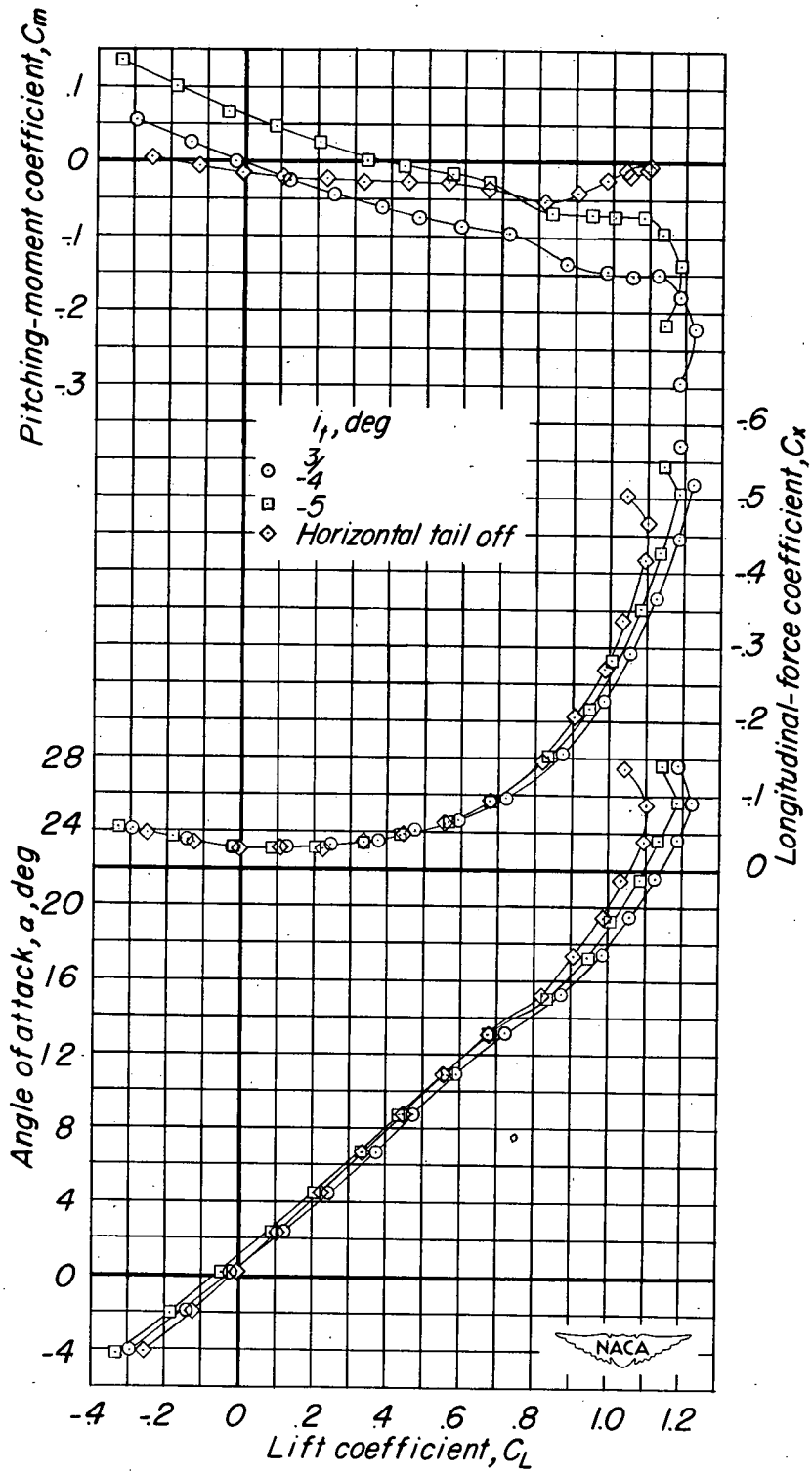

(c) $\Lambda = 50^{\circ}$.

Figure 7.- Continued.

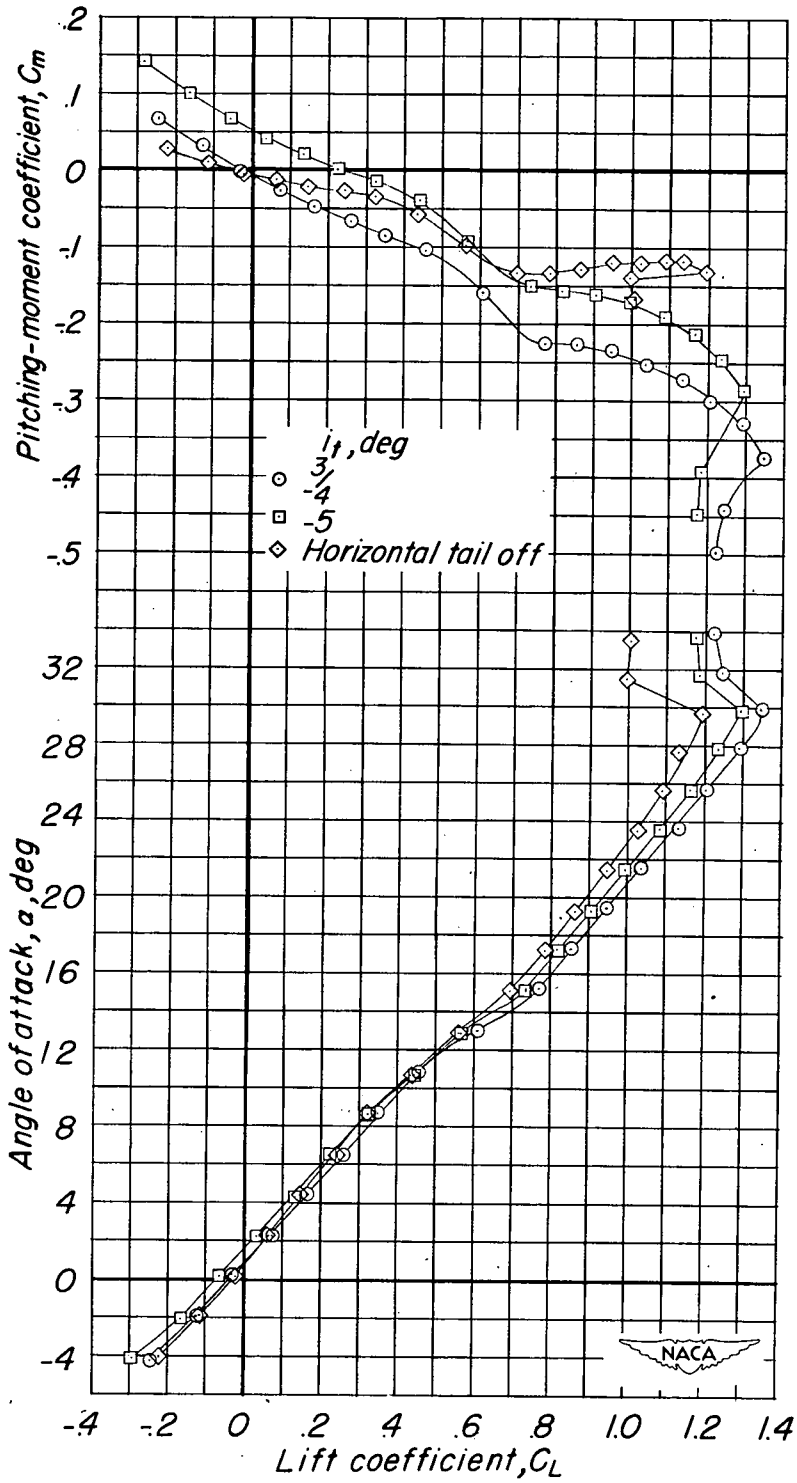

(d) $\Lambda = 60^{\circ}$.

Figure 7.- Continued.

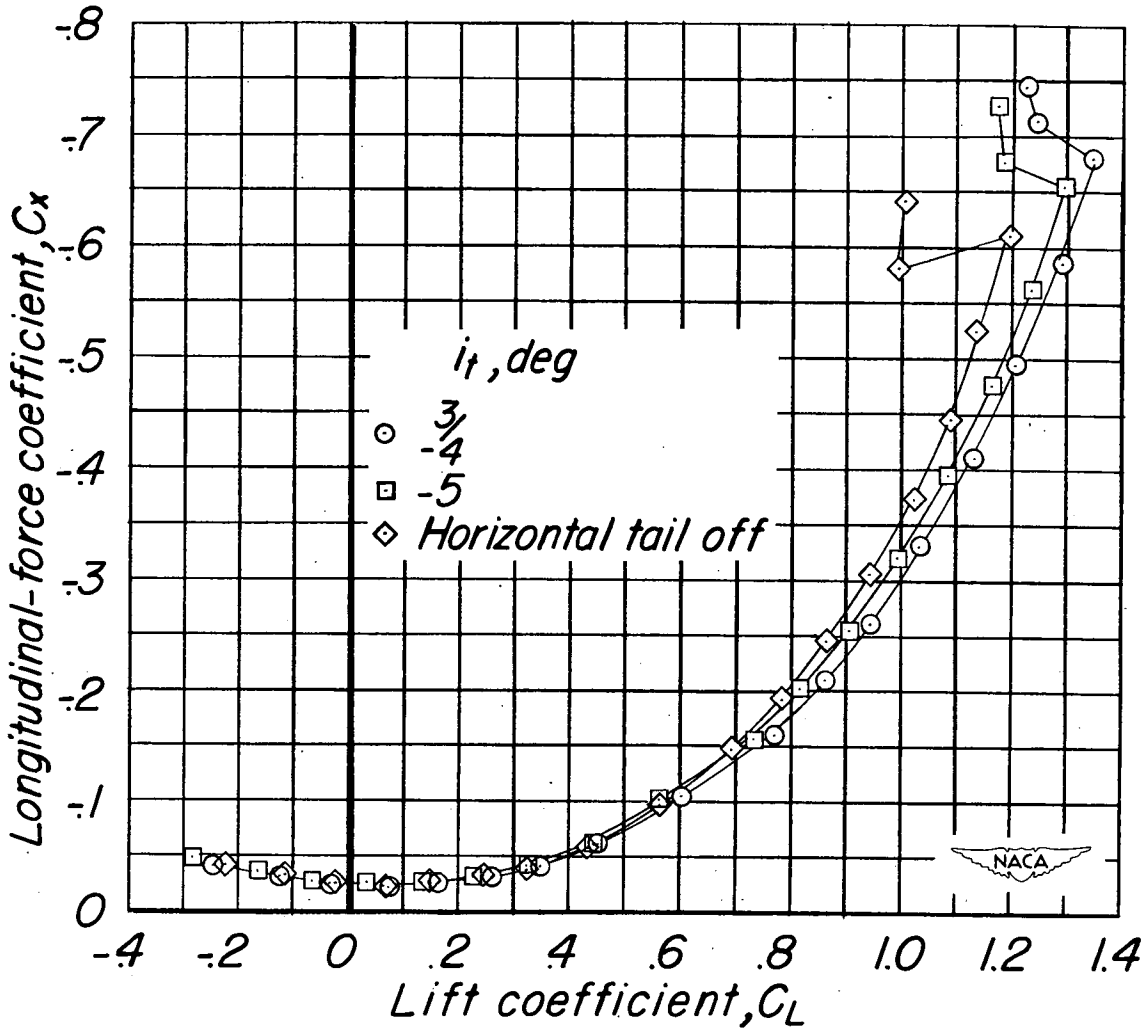

(d) Concluded.

Figure 7.- Concluded.

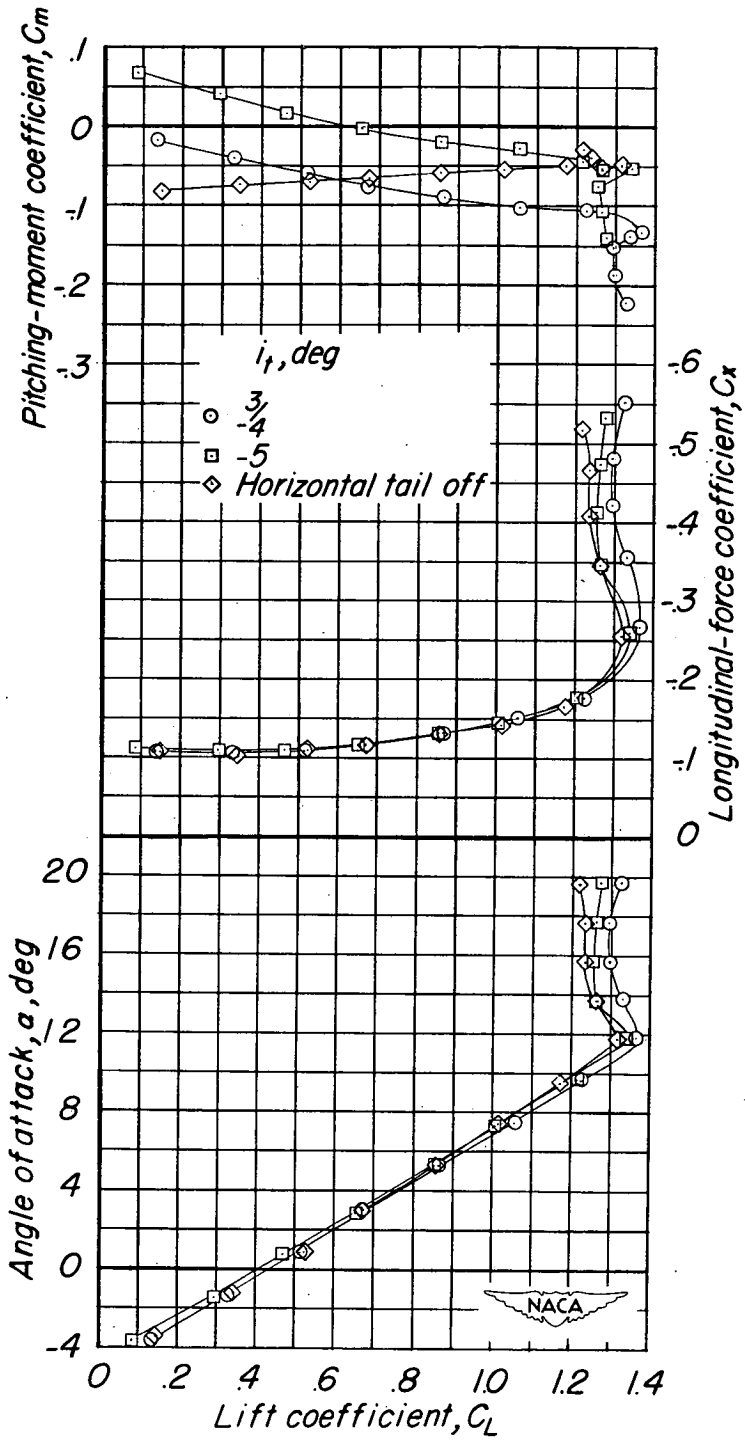

(a) Modification 1.

Figure 8.- Longitudinal aerodynamic characteristics of the model at 20° sweep with split flaps deflected 50°.

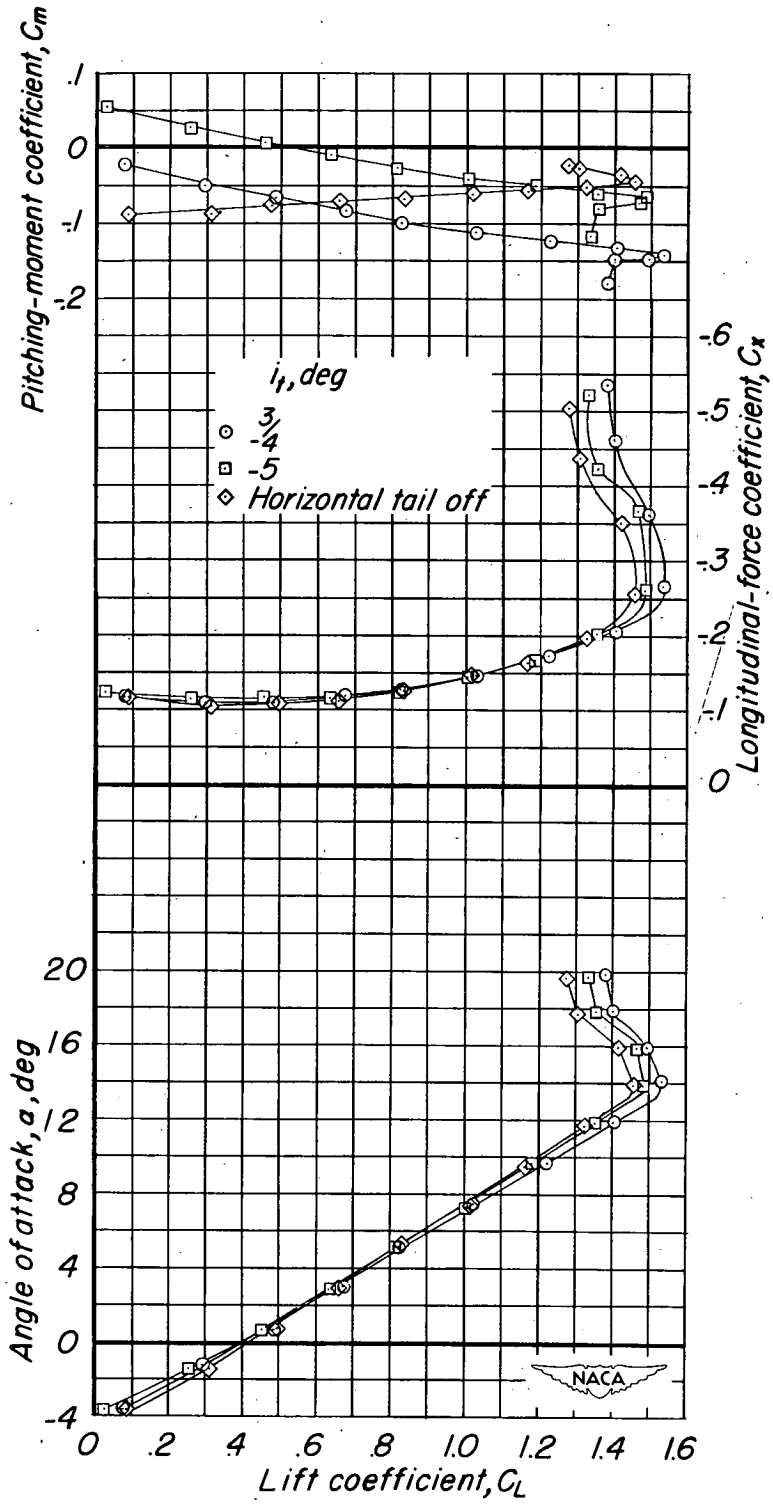

(b) Modification 2.

Figure 8.- Concluded.

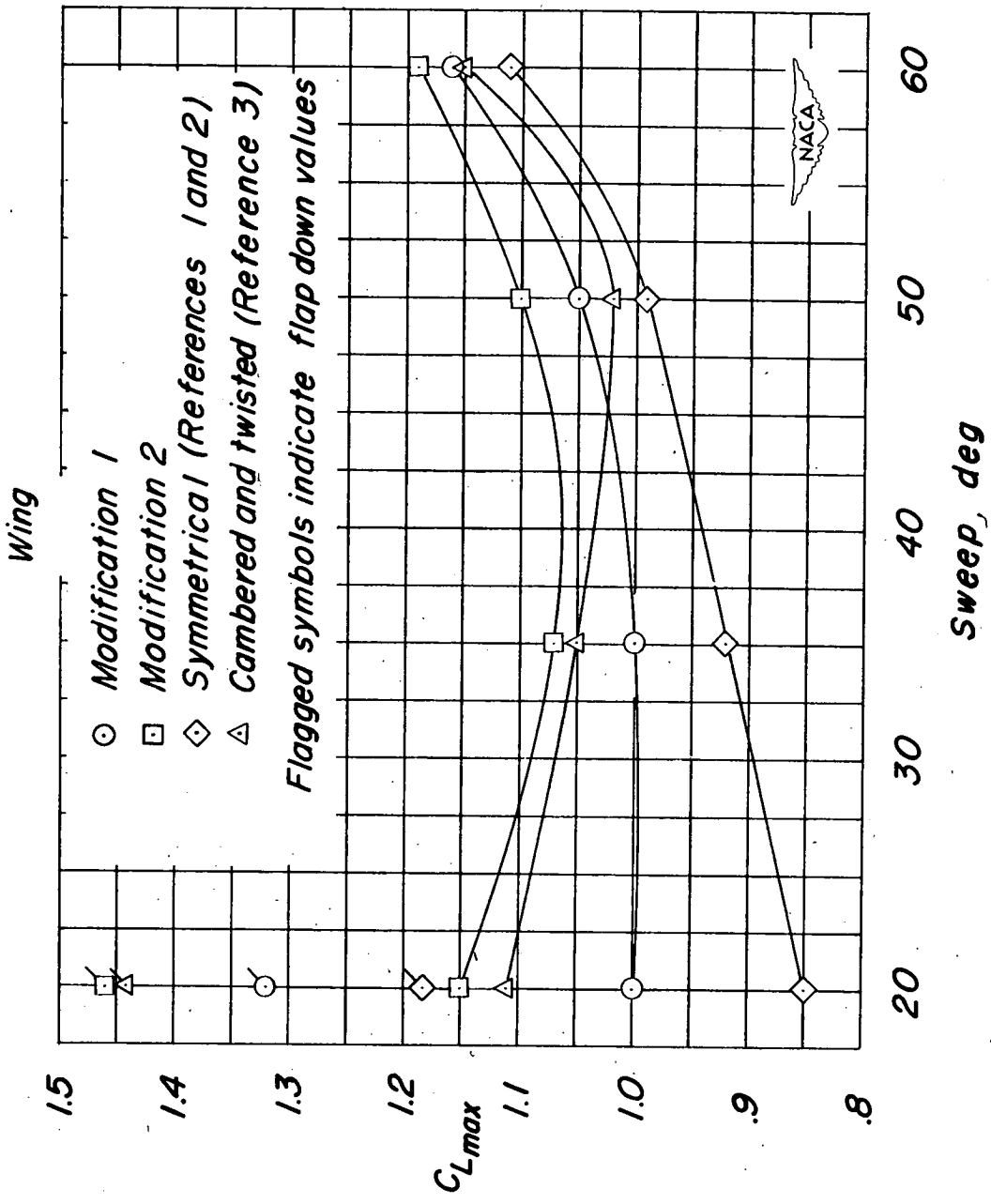

Figure 9.- The effect of the various wing modifications on the maximum lift coefficient for the wing-fuselage combination.

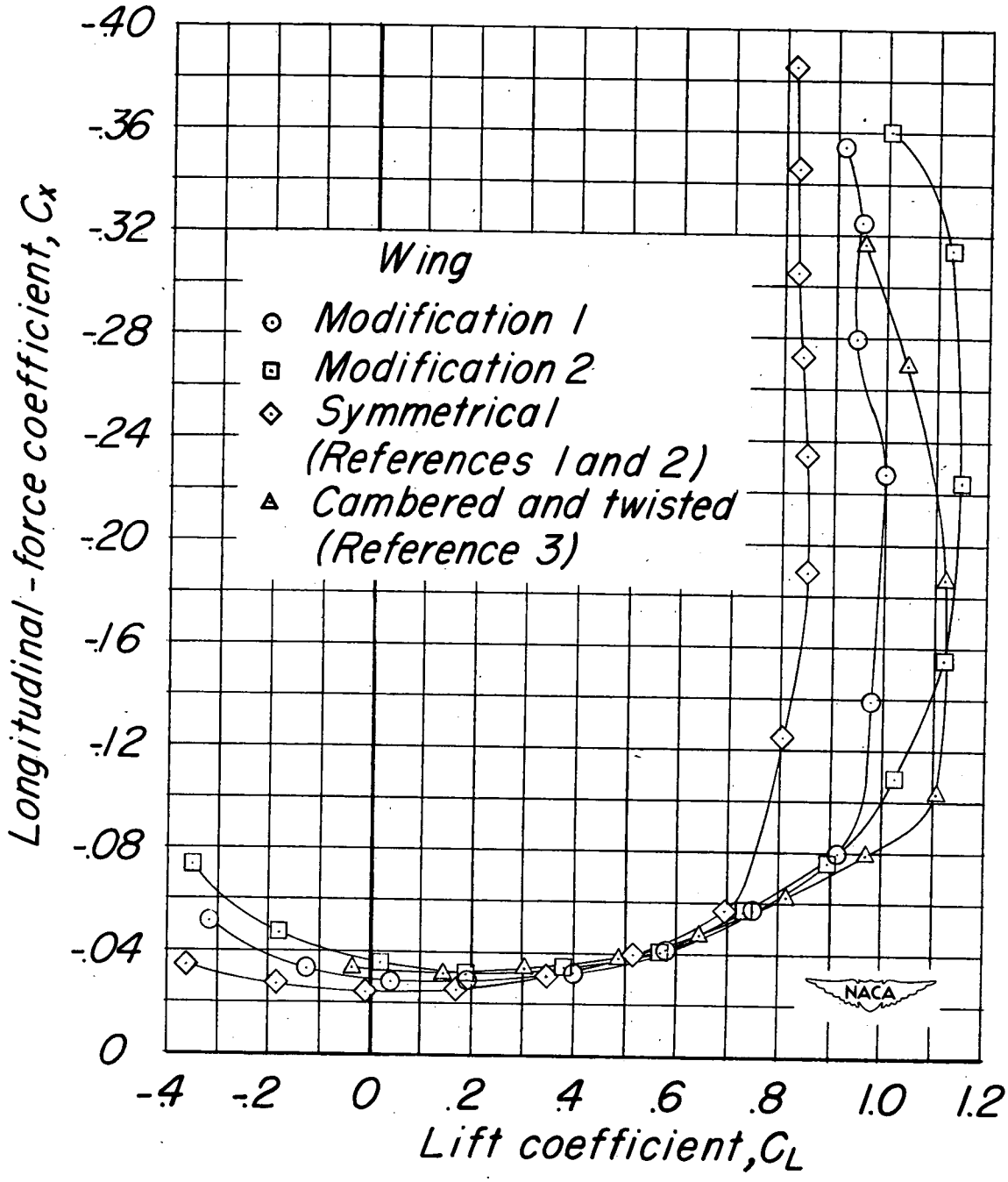

(a) $\Lambda = 20^{\circ}$.

Figure 10.- The effect of the various wing modifications on the drag characteristics of the wing-fuselage combination. $\delta_f = 0^{\circ}$.

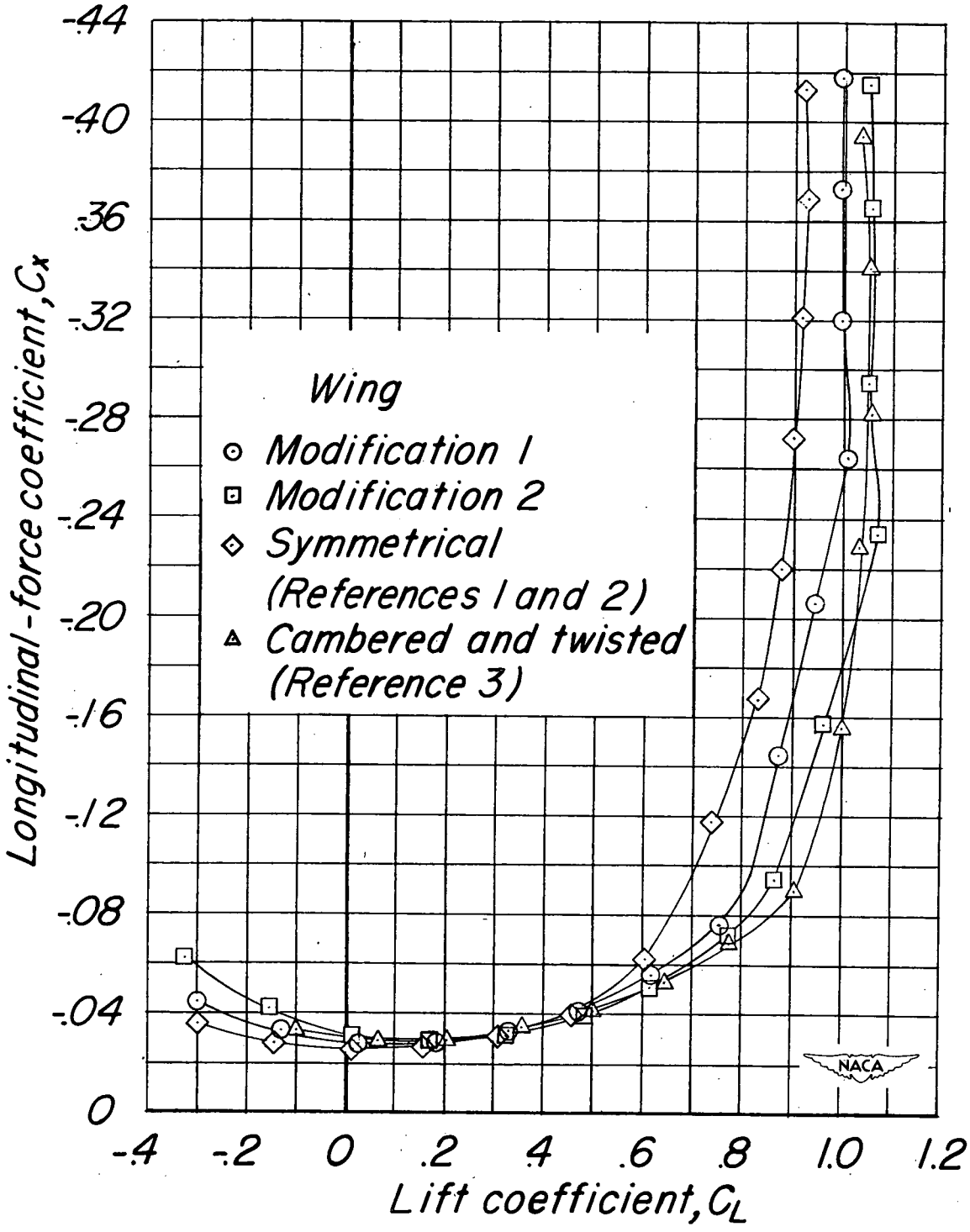

(b) $\Lambda = 35^{\circ}$.

Figure 10.- Continued.

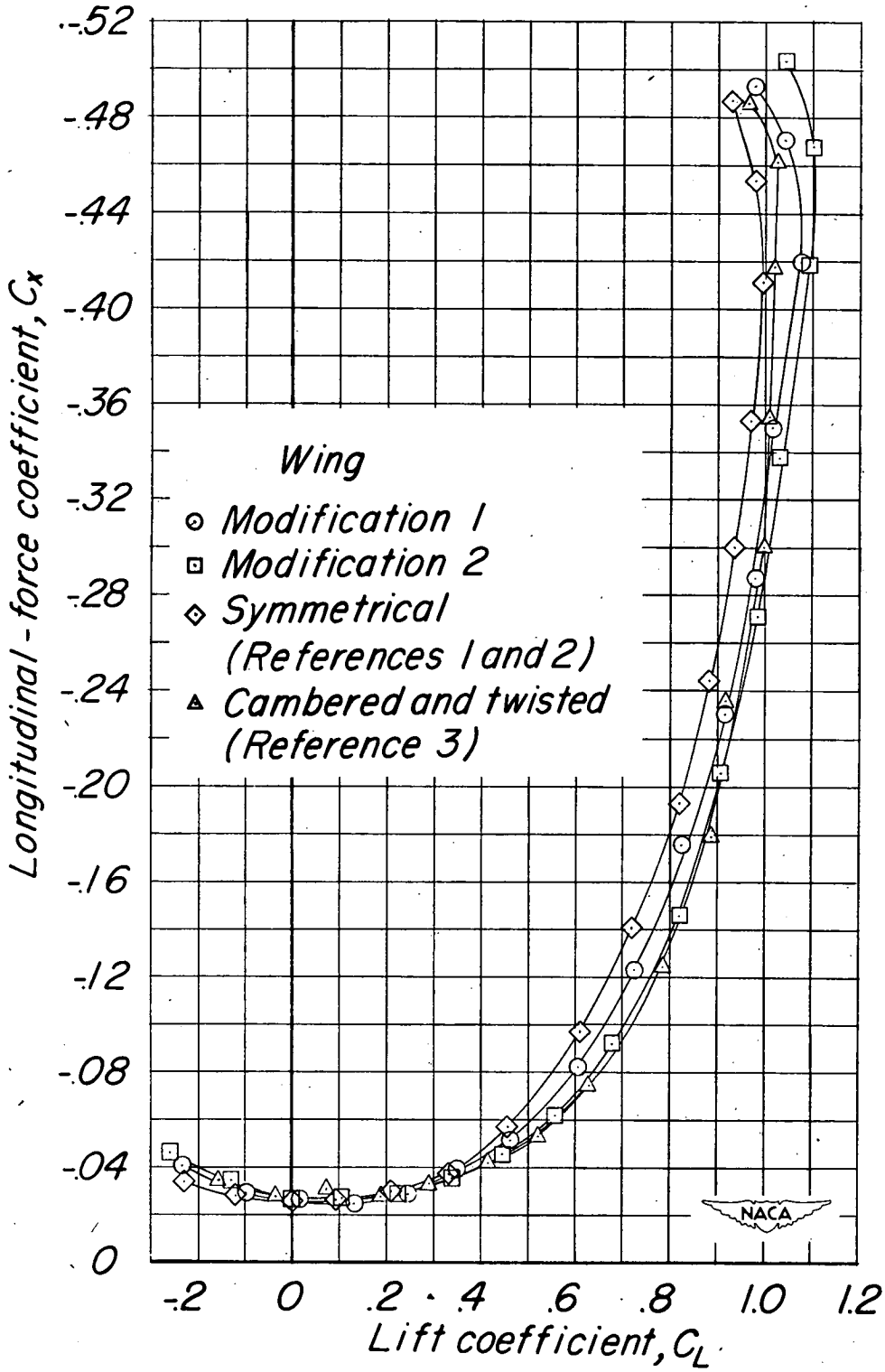

(c) $\Lambda = 50^{\circ}$.

Figure 10.- Continued.

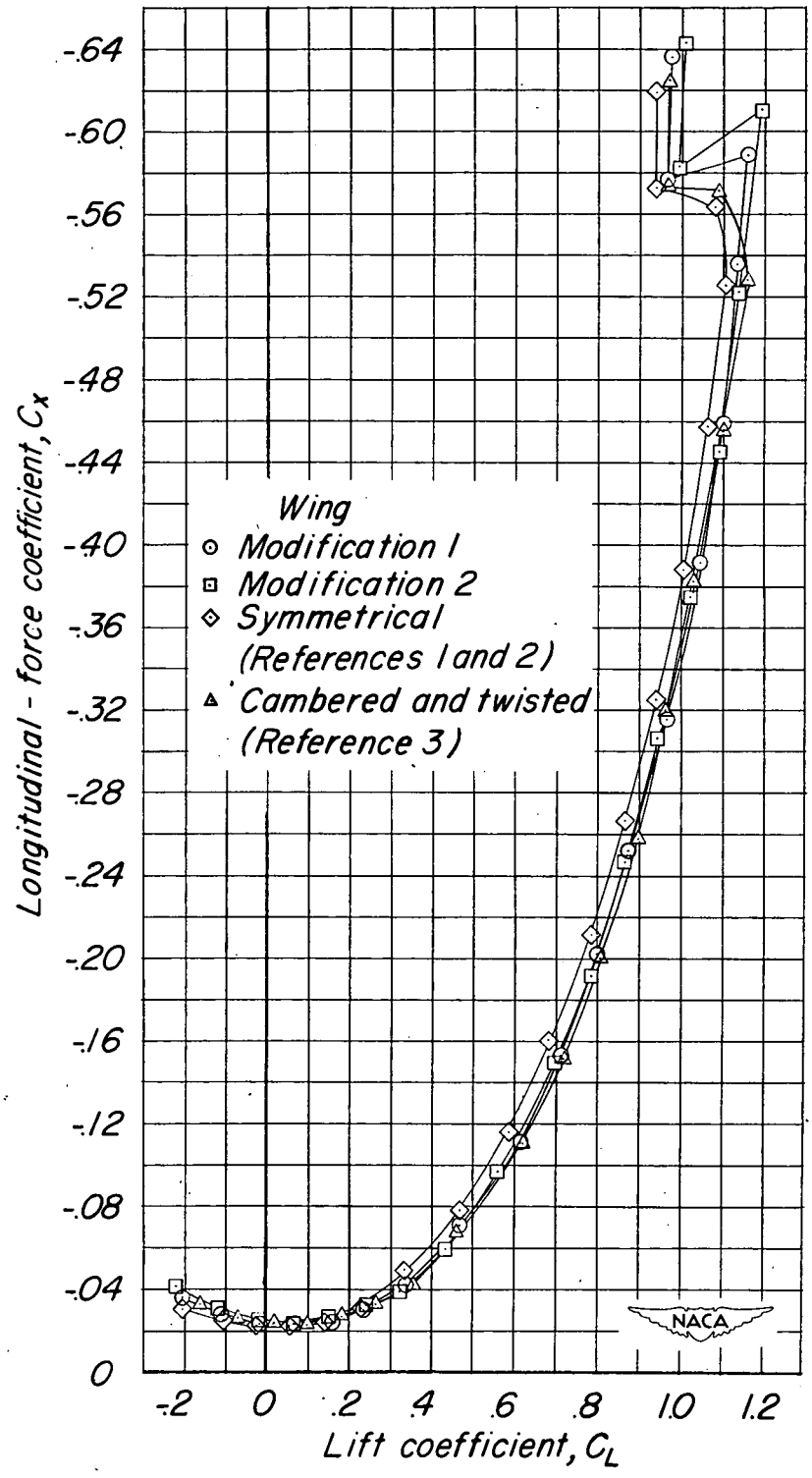

(d) $\Lambda = 60^{\circ}$.

Figure 10.- Concluded.

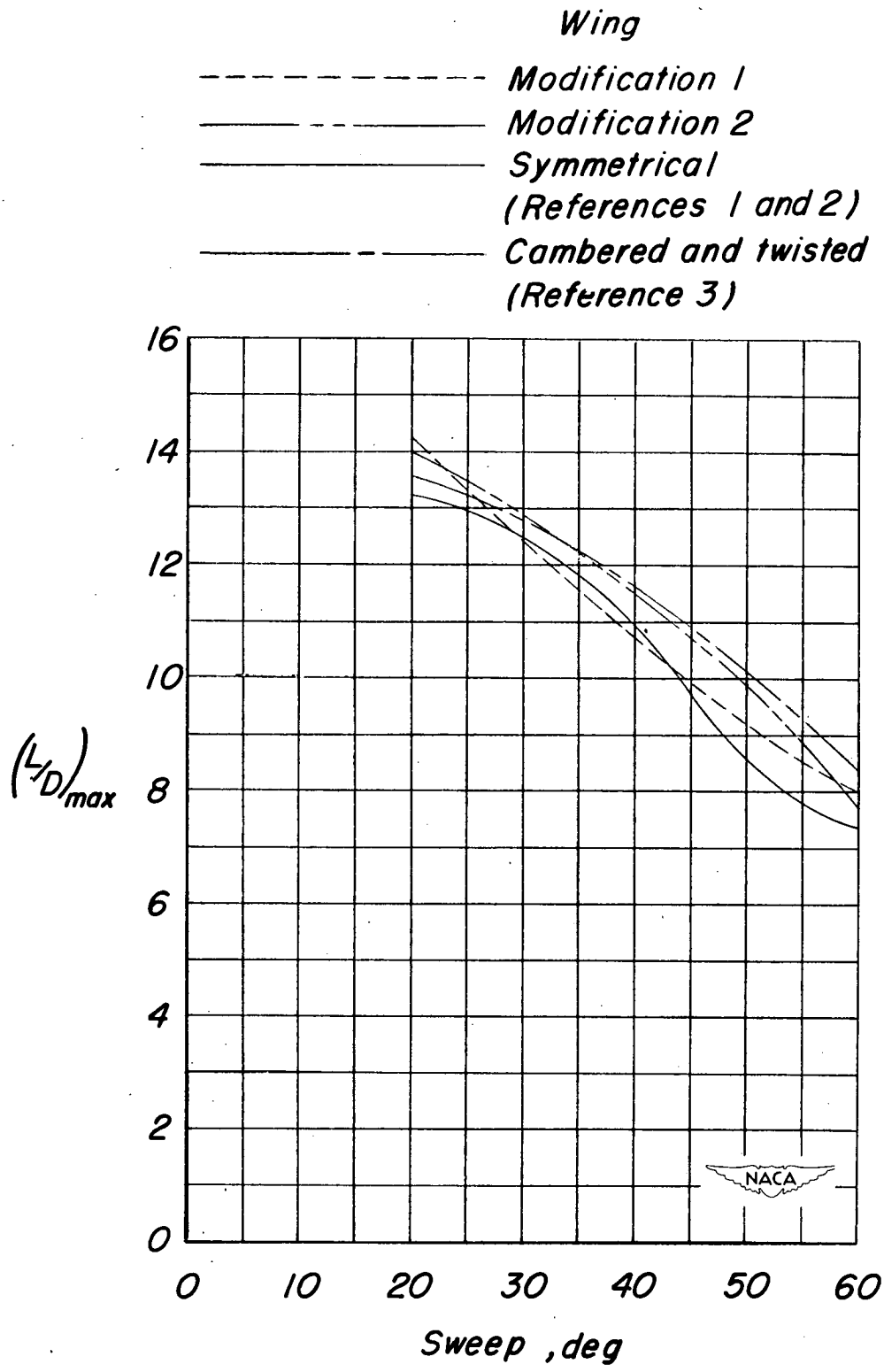

Figure 11.- The effect of the various wing modifications on the maximum lift-drag ratios of the wing-fuselage combination. $\delta_f = 0^{\circ}$.

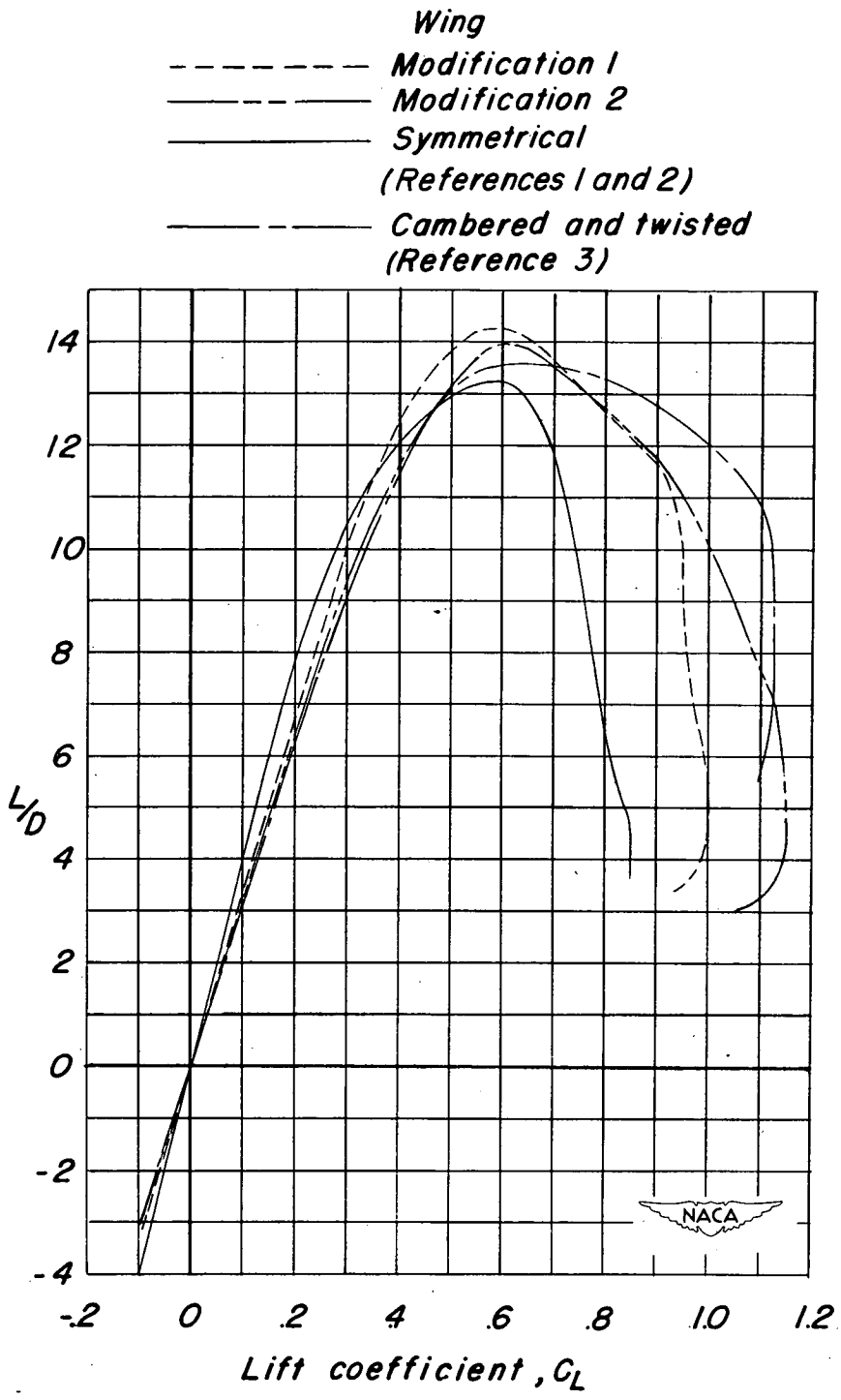

(a) $\Lambda = 20^{\circ}$.

Figure 12.- The effect of the various wing modifications on the lift-drag ratios of the wing-fuselage combination. $\delta_f = 0^{\circ}$.

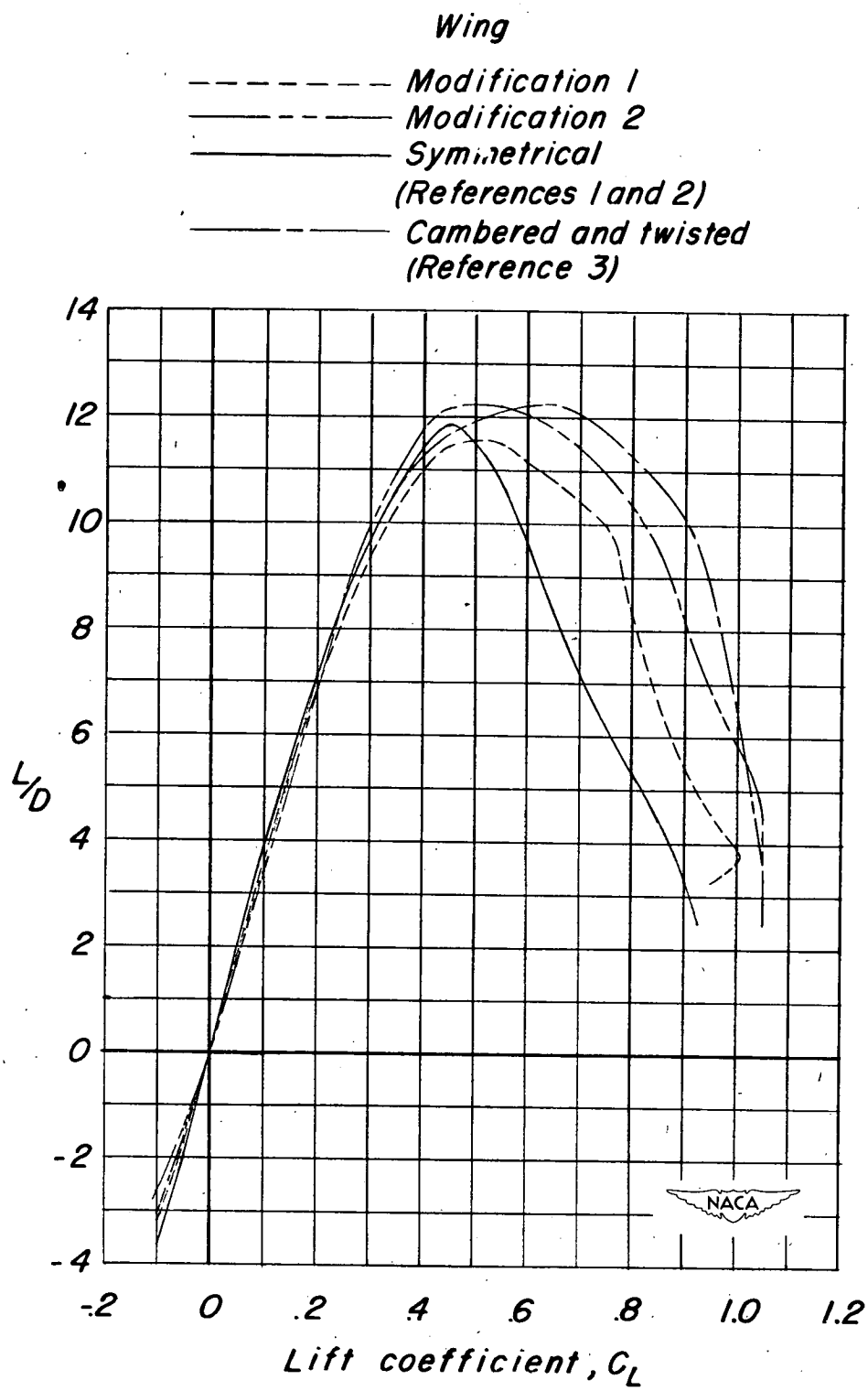

(b) $\Lambda = 35^{\circ}$.

Figure 12.- Continued.

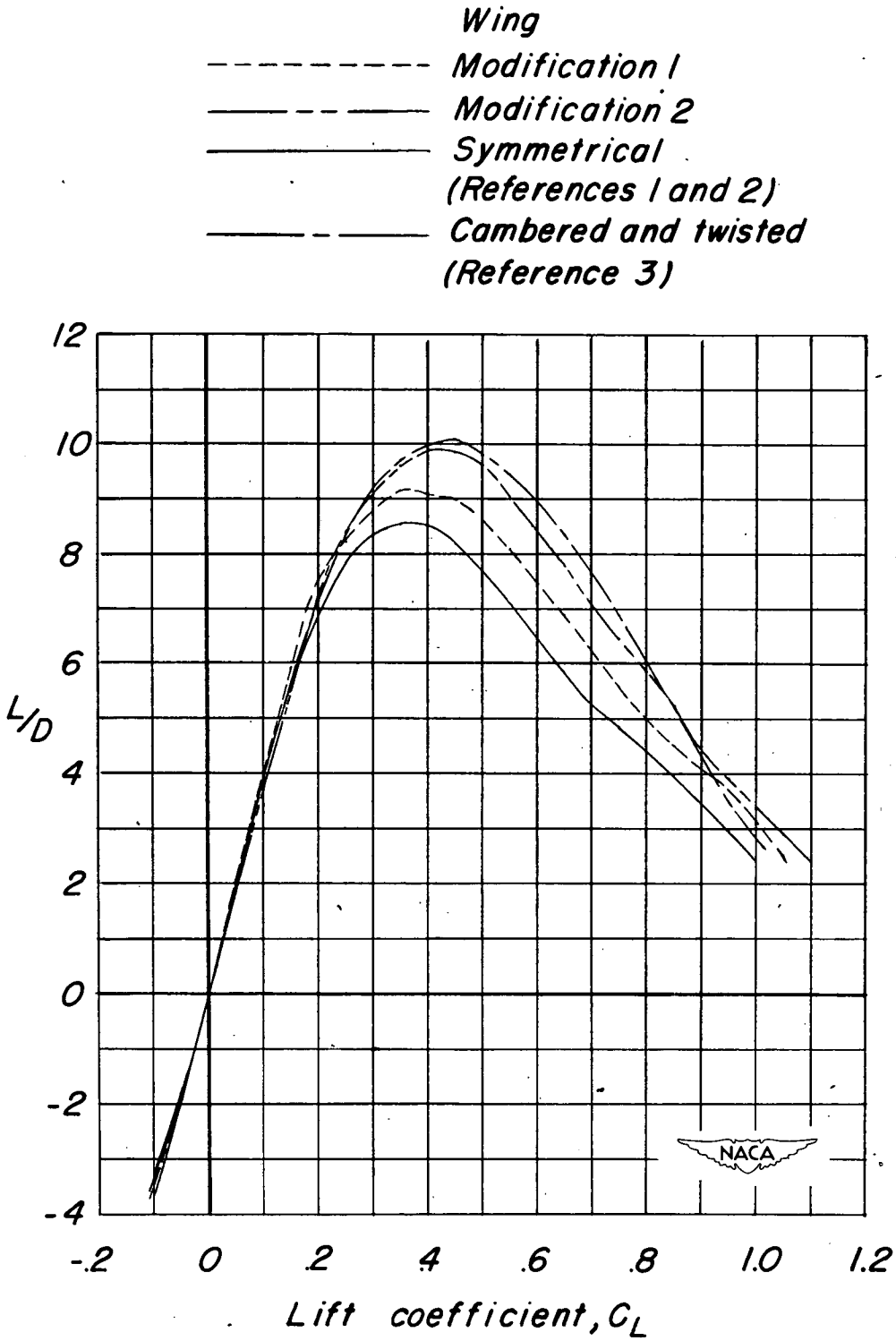

(c) $\Lambda = 50^{\circ}$.

Figure 12.- Continued.

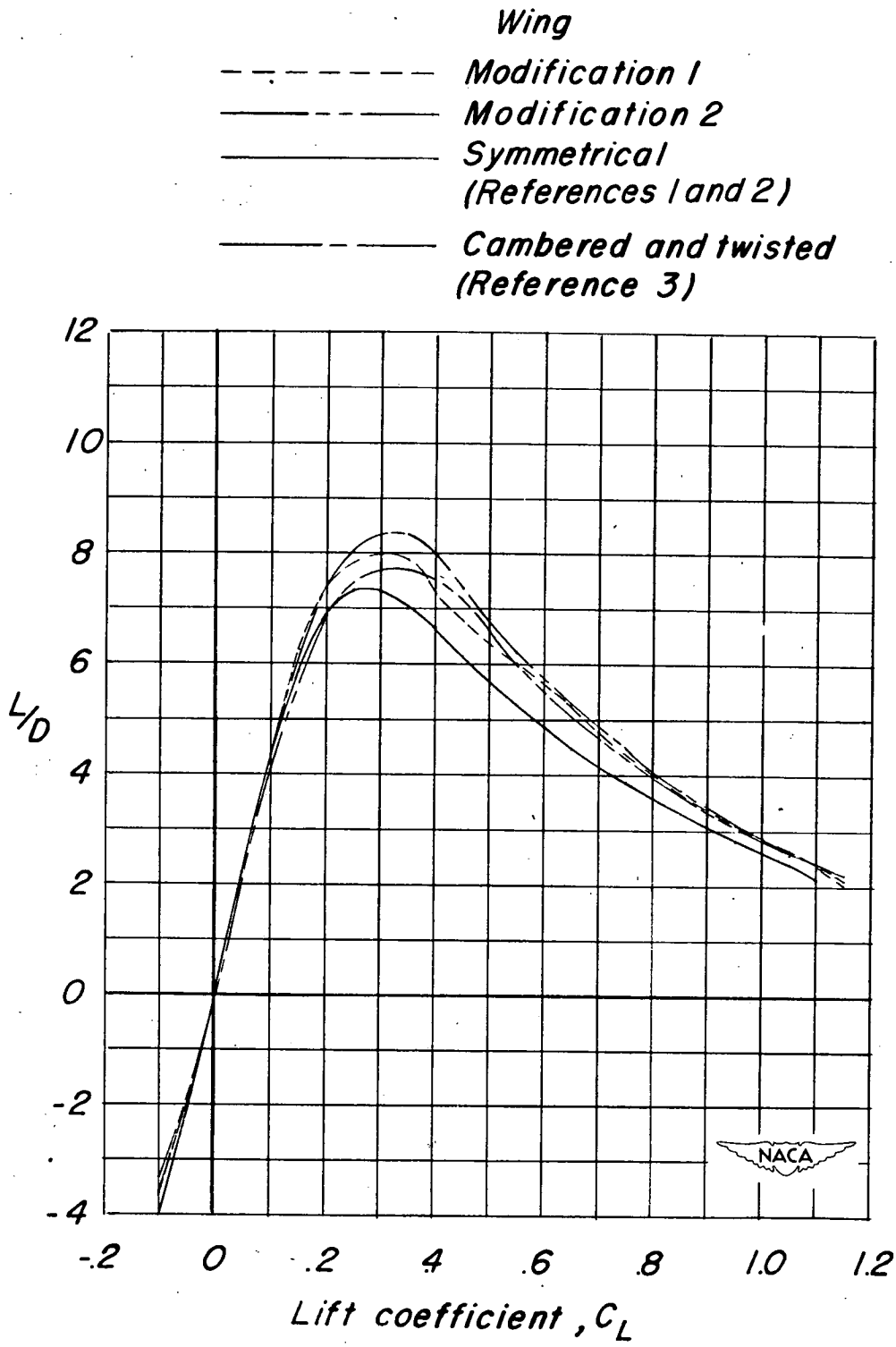

(d) $\Lambda = 60^{\circ}$.

Figure 12.- Concluded.

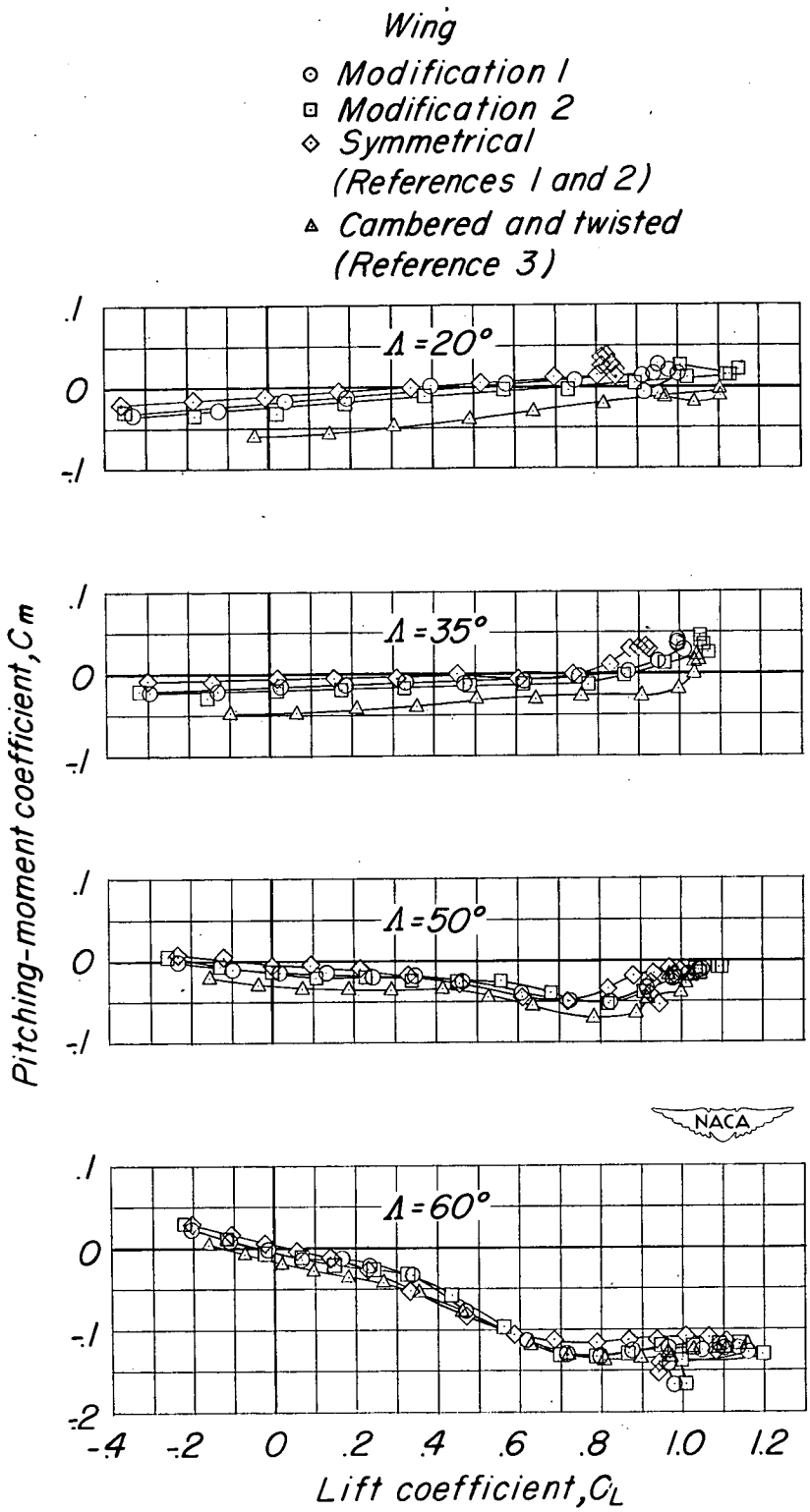

Figure 13.- The effect of the various wing modifications on the pitching-moment characteristics of the wing-fuselage combination. $\delta_f = 0$.

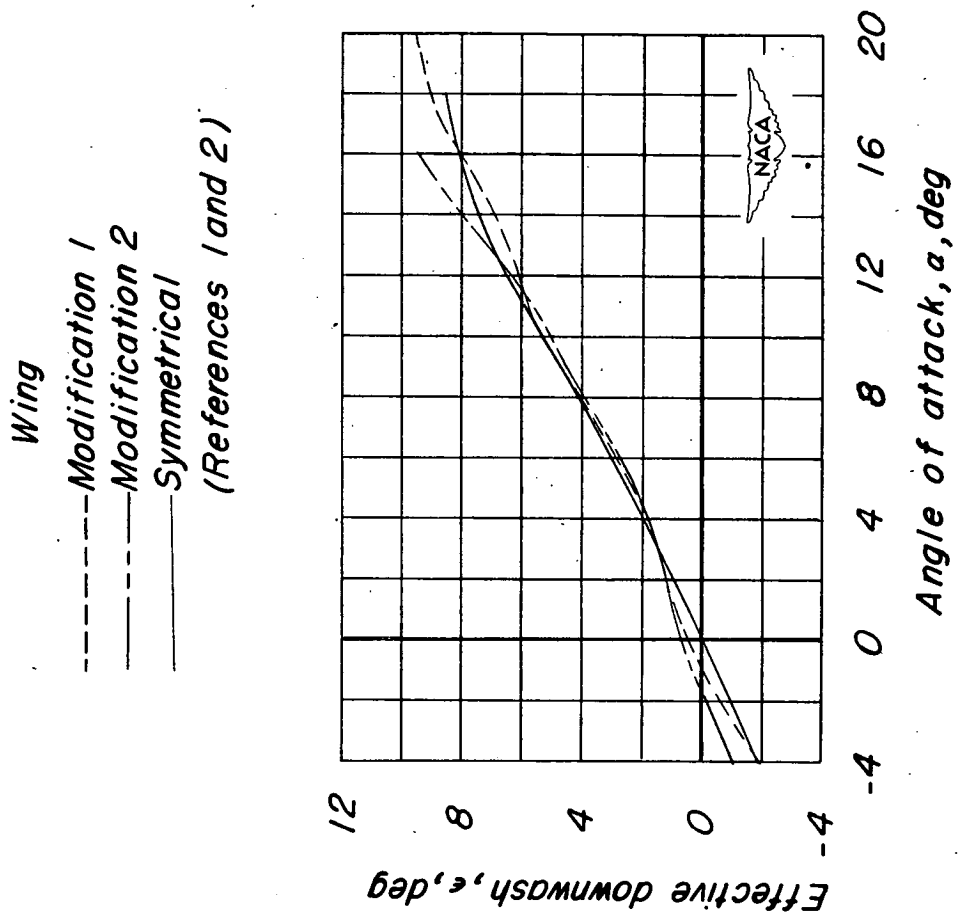

(a) $\Lambda = 20^{\circ}$.

Figure 14.- The effect of the various wing modifications on the effective downwash at the tail of the test model. $\delta_f = 0$.

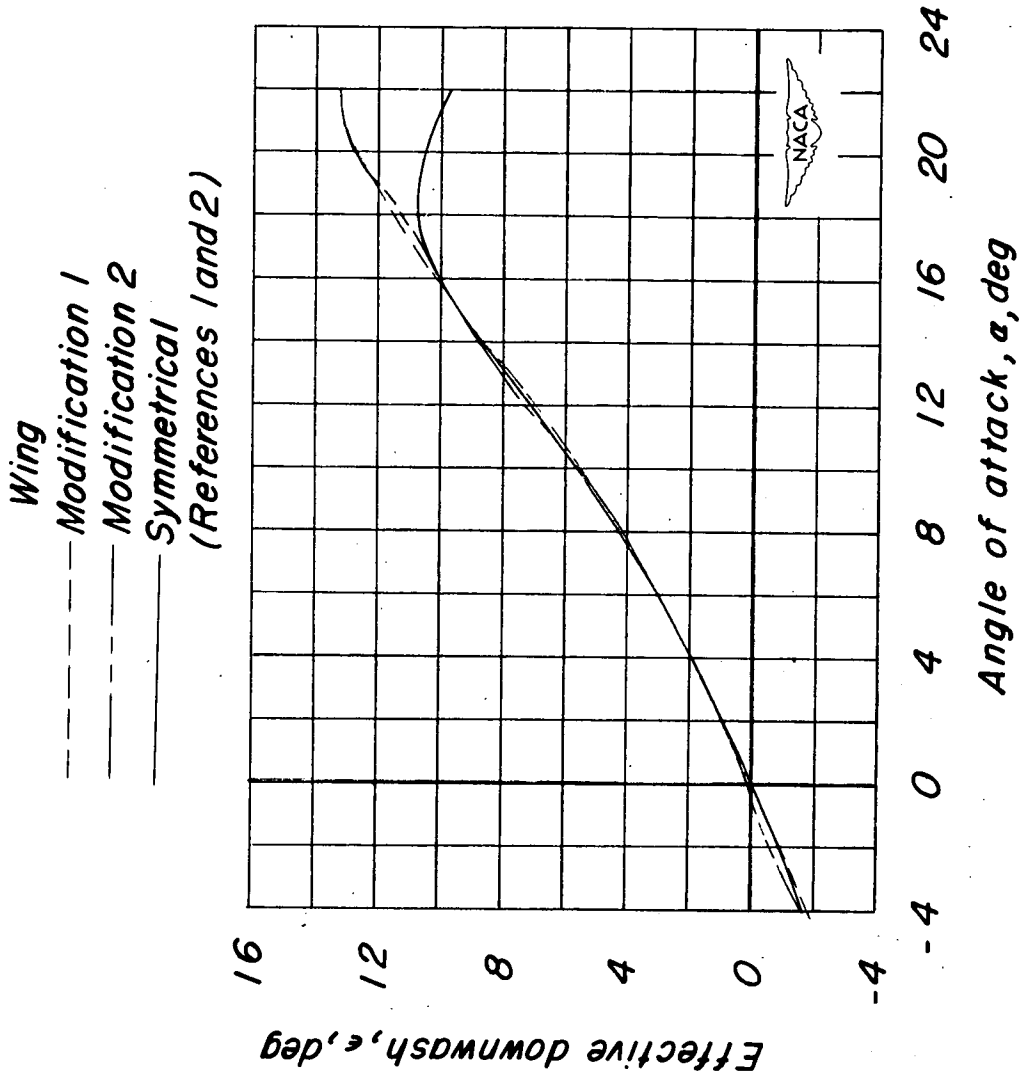

(b) $\Lambda = 35^{\circ}$.

Figure 14.- Continued.

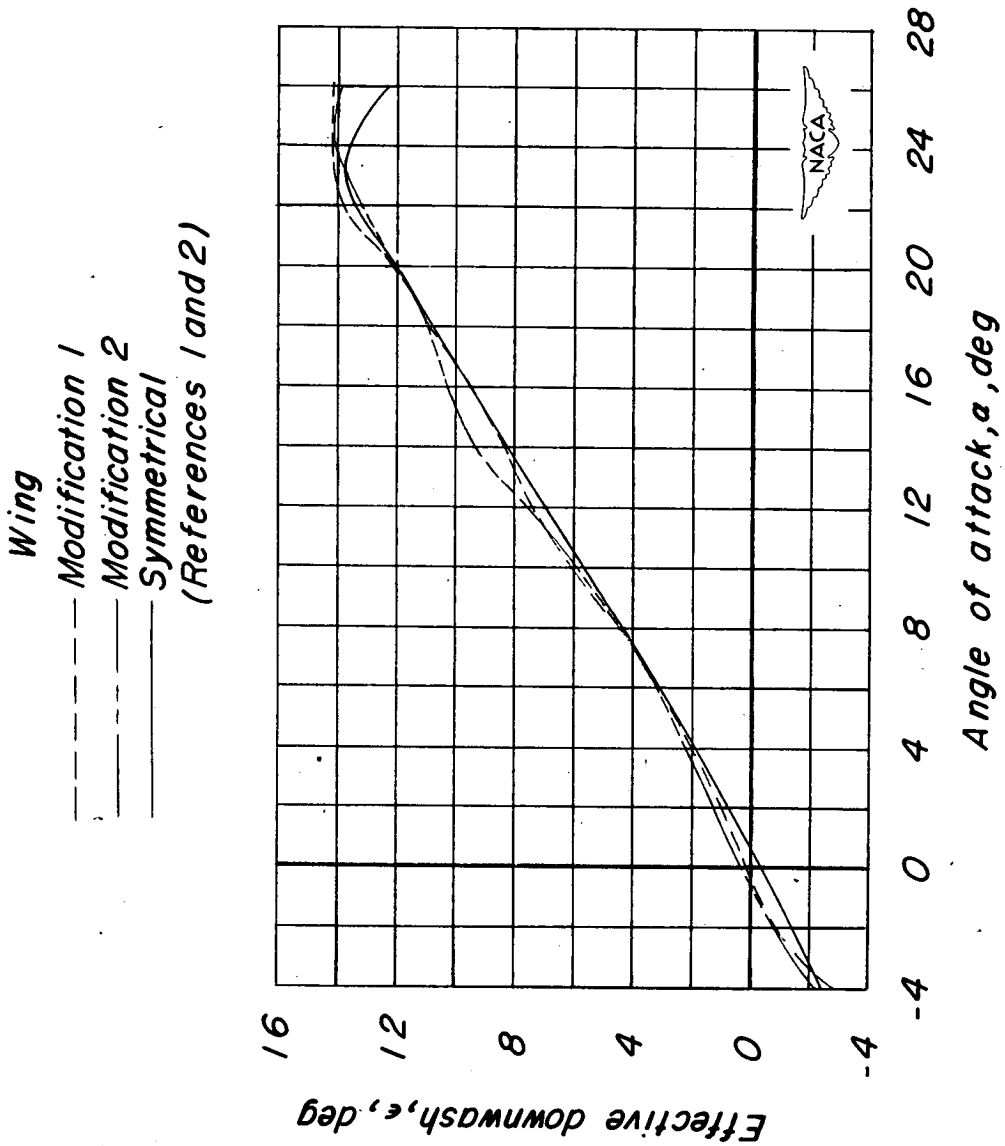

(c) $\Lambda = 50^{\circ}$.

Figure 14.- Continued.

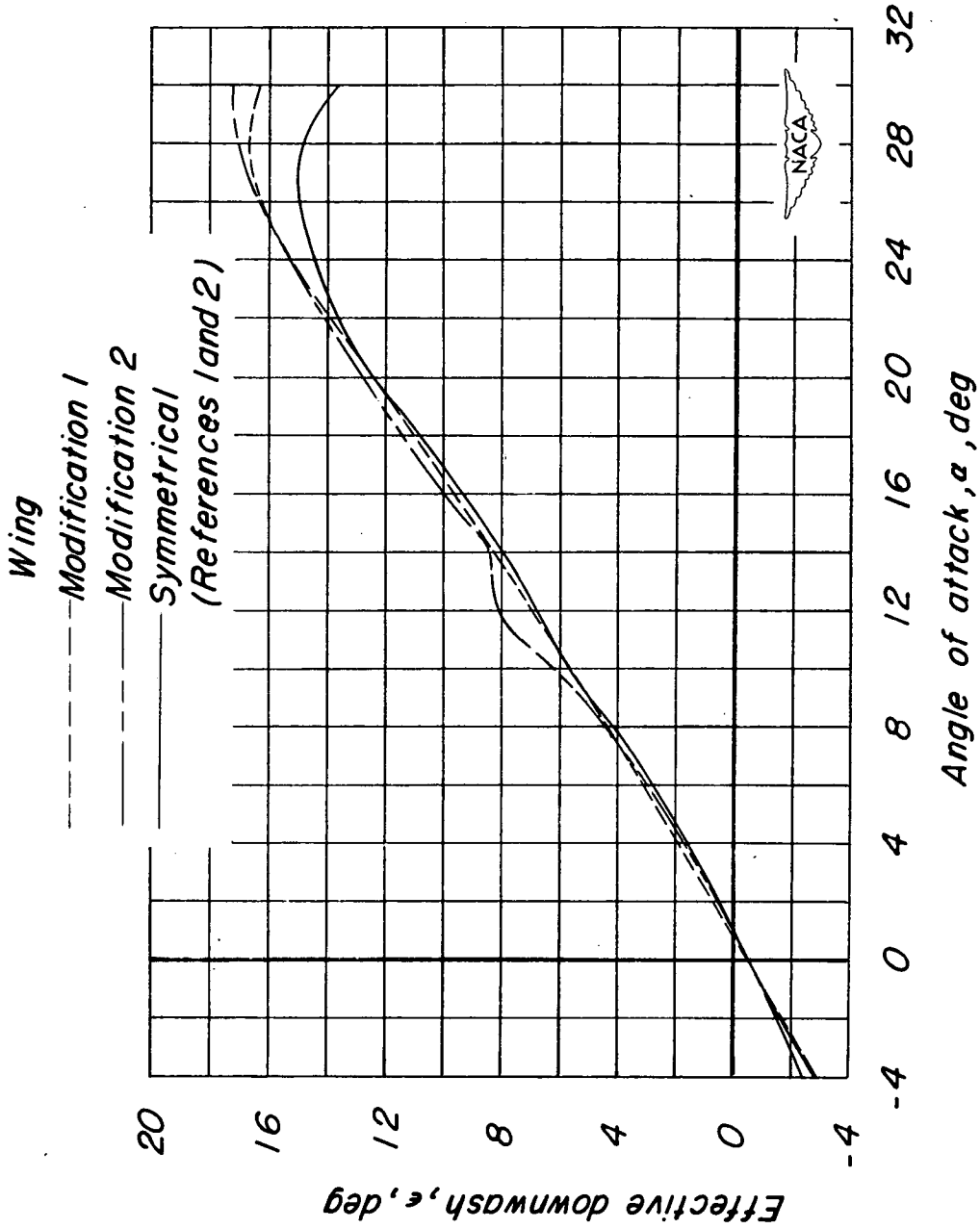

(d) $\Lambda = 60^{\circ}$.

Figure 14.- Concluded.

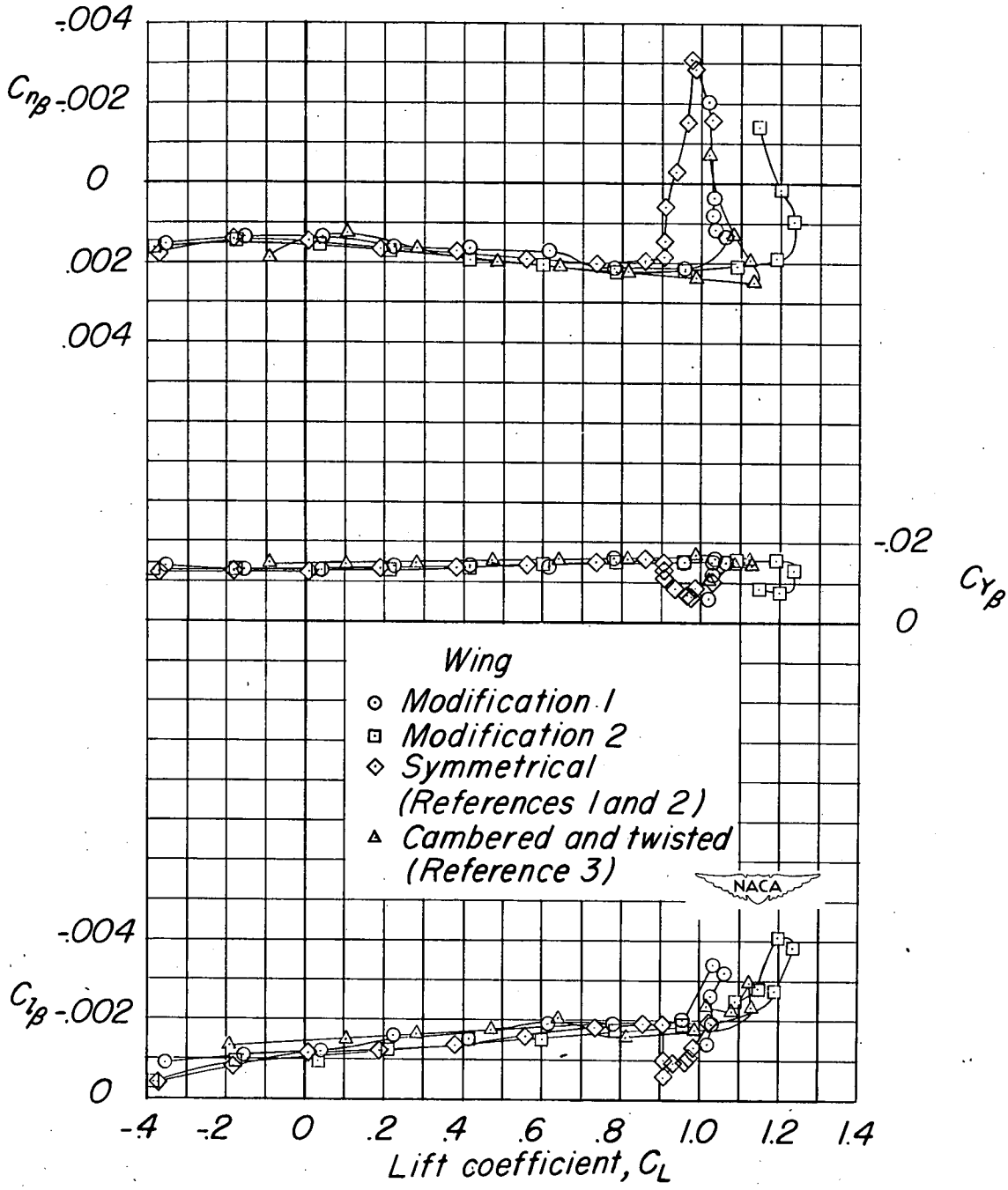

(a) $\Lambda = 20^{\circ}$.

Figure 15.- The effect of the various wing modifications on the static-lateral-stability parameters of the test model. $i_t = -\frac{3^{\circ}}{4}$; $\delta_f = 0$.

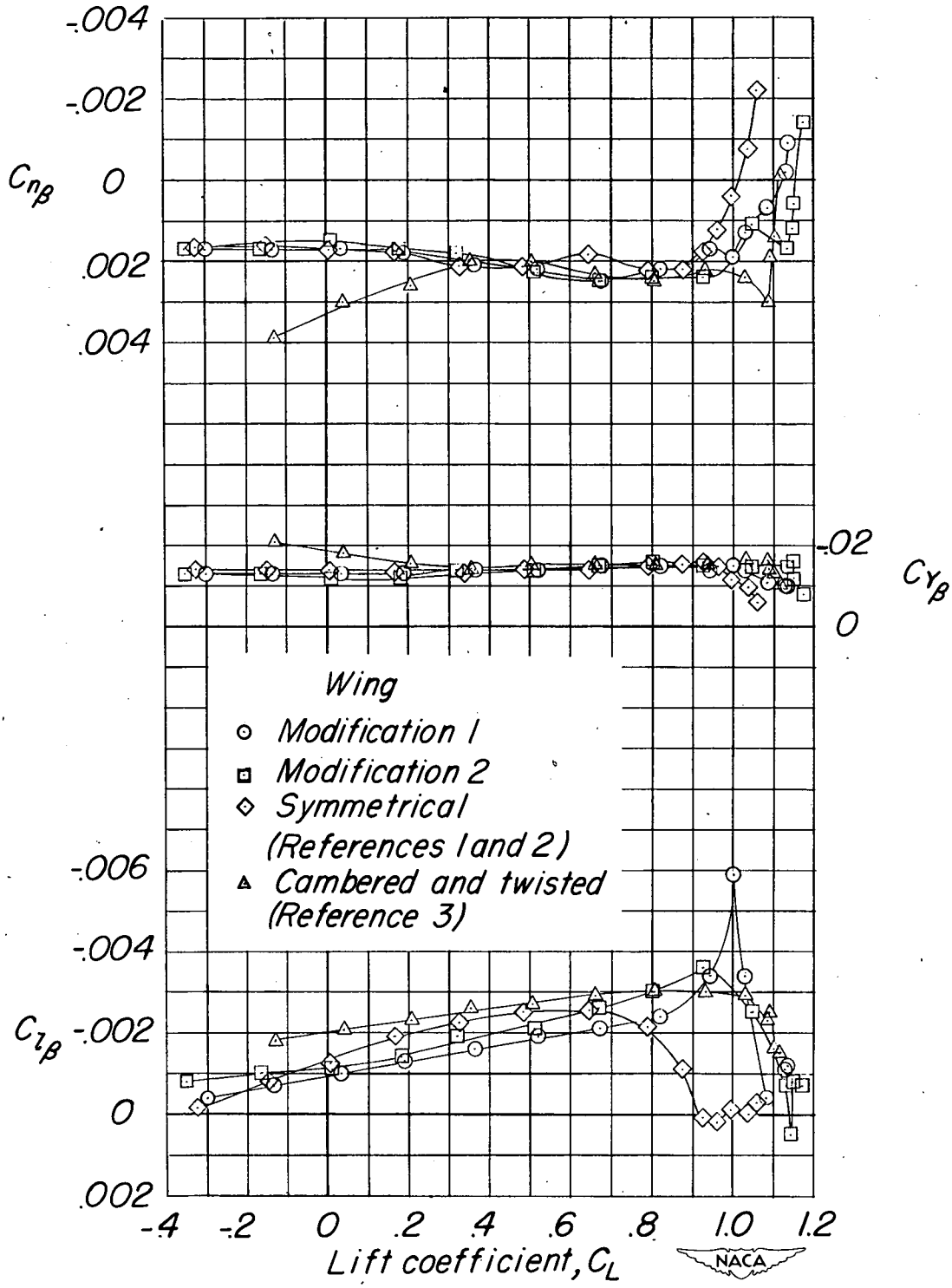

(b) $\Lambda = 35^{\circ}$.

Figure 15.- Continued.

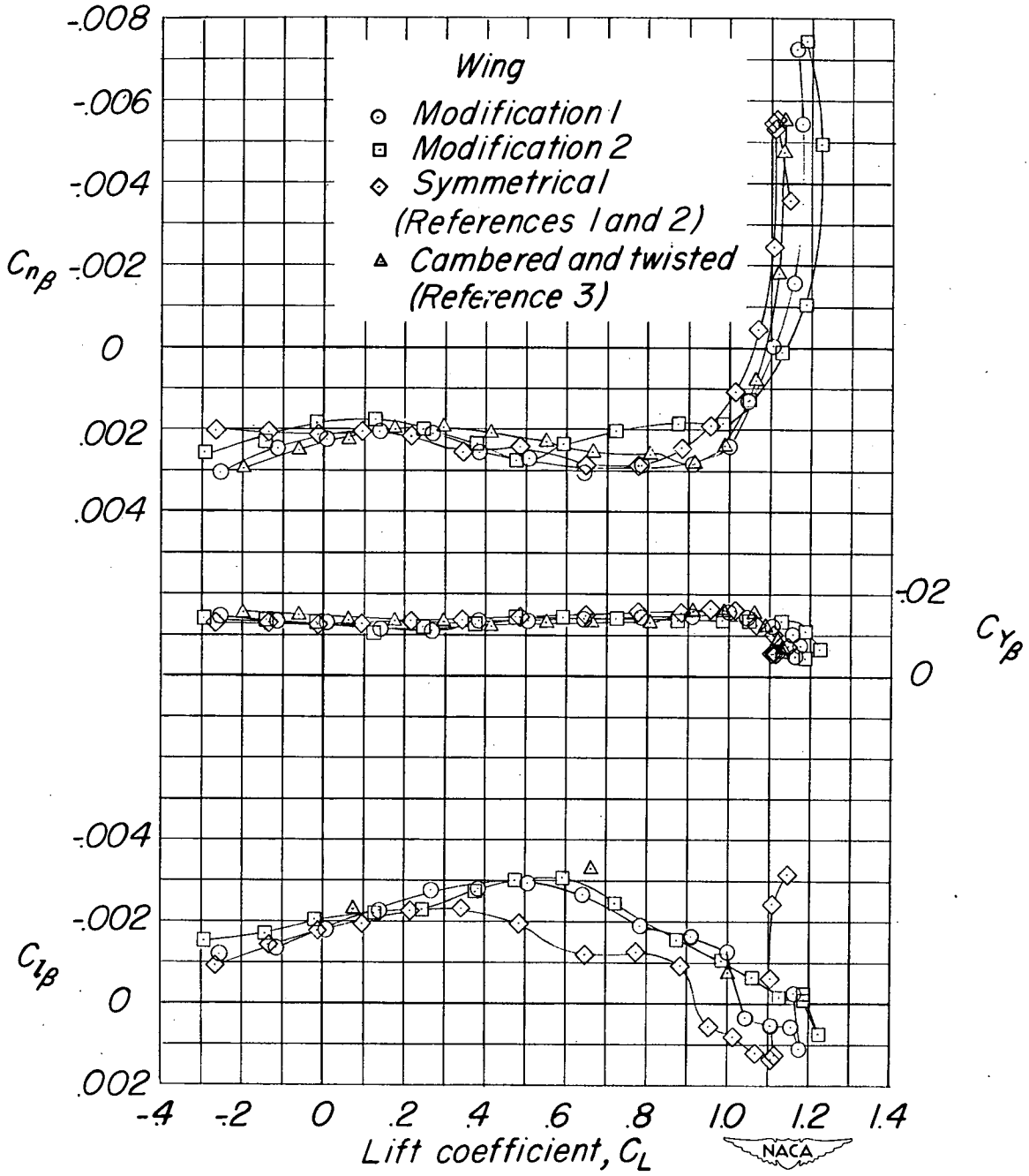

(c) $\Lambda = 50^{\circ}$.

Figure 15.- Continued.

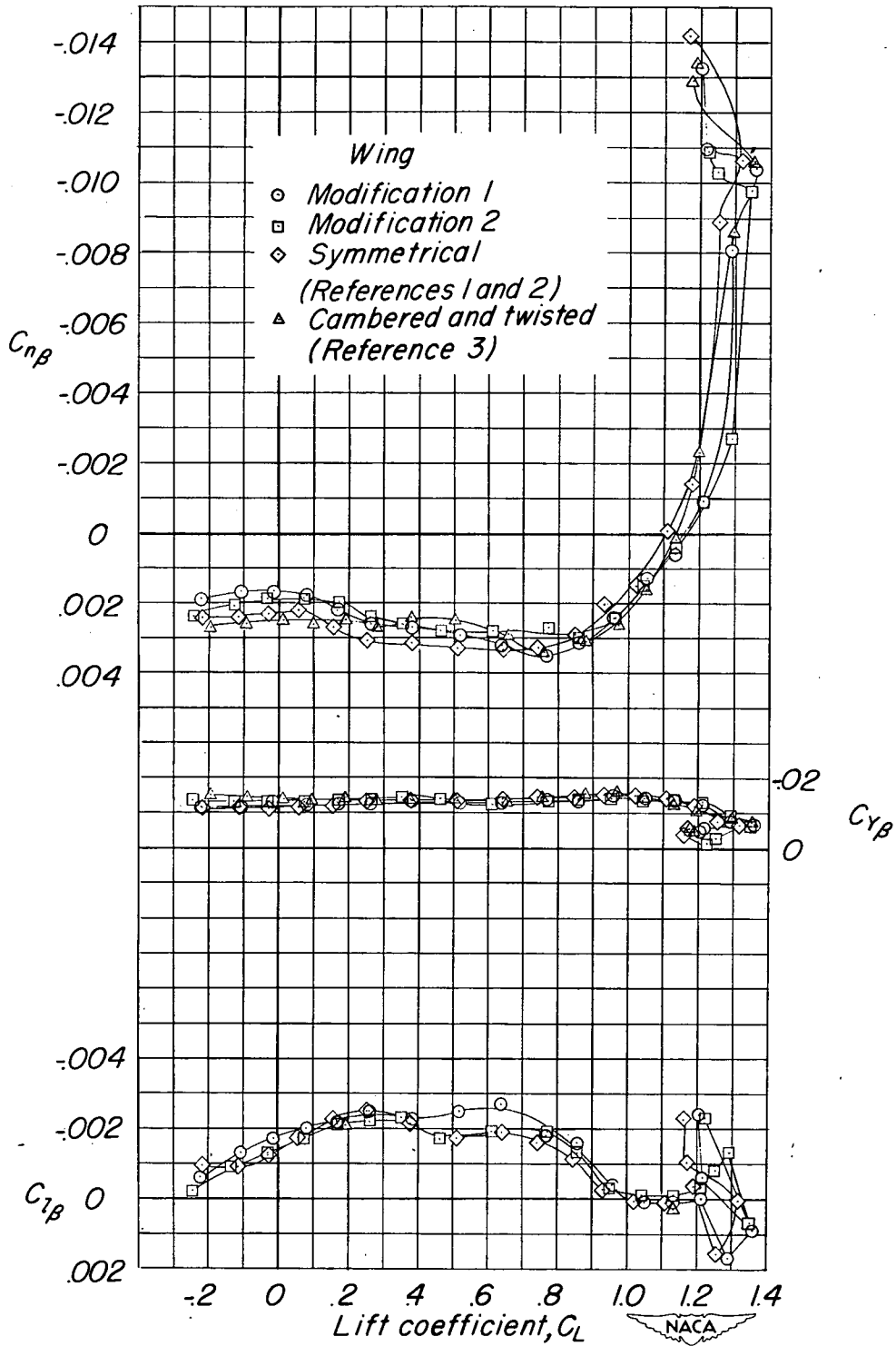

(d) $\Lambda = 60^{\circ}$.

Figure 15.- Concluded.